SMALL NUCLEOLAR RNA EXPRESSION AND NADPH OXIDASE-MEDIATED ROS PRODUCTION IN THP-1 MACROPHAGES TREATED WITH VLDL HYDROLYSIS PRODUCTS

Mariam Olanrewaju TIJANI, B.Sc., M.Sc.

A thesis submitted to the School of Graduate Studies in partial fulfillment of the requirements for the degree of

Master of Science

Department of Biochemistry, Faculty of Science

Memorial University of Newfoundland

May 2025

St. John’s, Newfoundland and Labrador

Abstract

One of the fundamental pathogenetic processes of atherosclerosis, oxidative stress, is defined by an increase in reactive oxygen species (ROS) generation. An increase in ROS production and oxidative stress have been linked to the expression of some specific kinds of snoRNAs. NADPH oxidase (NOX) appears to play a role in regulating snoRNA expression and snoRNA accumulation in the cell cytosol. Our laboratory previously reported an upregulation of 63 snoRNA transcripts in macrophages incubated with lipoprotein (Lp) lipid hydrolysis products (HPs) generated by lipoprotein lipase (LPL). I hypothesized that Lp HPs produced by LPL lead to NOX-mediated oxidative stress within THP-1 macrophages that can be inhibited using the NADPH oxidase inhibitors (NOXi) apocynin or GKT136901. I further hypothesized that snoRNA expression would increase due to NOX activity in macrophages incubated with Lp hydrolysis products by LPL. My results show significant NOX-induced ROS production, using cellular ROS detection assay, in differentiated THP-1 macrophages treated with very low-density lipoprotein (VLDL) HPs by LPL. The NOX-induced ROS production was inhibited by 20 μM of GKT136901, while 100 μM of apocynin had no inhibitory effect. The NOX-induced ROS did not induce lipid peroxidation in the macrophages. RNA integrity numbers (RIN) were analyzed using an RNA bioanalyzer, with no significant alteration in the RIN of the total RNA isolated from the THP-1 macrophages treated with 0.25 mM VLDL HPs. The NOX-induced ROS also did not alter the expression of *SNORA56, SNORA60*, and *SNORA80E* in the VLDL HP-treated macrophages. Overall, NOX-induced ROS production seems not to mediate the overexpression of *SNORA56, SNORA60*, and *SNORA80E* in PMA-differentiated THP-1 macrophages treated with 0.25 mM VLDL HPs by LPL.

Acknowledgments

I would begin by thanking my supervisor, Dr. Robert Brown, for his patience, unwavering guidance, and rich support throughout my program. I would also like to thank my supervisory committee members, Dr. Mark Berry and Dr. Valerie Booth, for their advice, insightful contributions, and thorough review of my research. I am grateful to our lab's astute research assistant, Elizabeth Chia, and my great lab mate, Kandeepan Karthigesu, for their invaluable technical assistance during this research. Finally, I want to thank my husband, Ayodeji Tinko, family, and friends, who supported me throughout the program. Thank you all.

Table of Contents

List of Tables

List of Figures

List of Abbreviations

A/A	Antibiotic/antimycotic
ABCA1	ATP-binding cassette transporter A1
Akt	Protein kinase B
apo	Apolipoprotein
ATCC	American Type Culture Collection
ATP	Adenosine triphosphate
BSA	Bovine serum albumin
CD36	Cluster of differentiation 36
CM	Chylomicron
CVD	Cardiovascular disease
DMEM	Dulbecco's Modified Eagle Medium
DMSO	Dimethyl sulfoxide
DNA	Deoxyribonucleic acid
EC	Endothelial cell
EDTA	Ethylenediaminetetraacetic acid
FAF	Fatty acid-free
FATP1	Fatty acid transport protein
FBS	Fetal bovine serum
FFA	Free fatty acid
GTP	Guanosine-5'-triphosphate
HAEC	Human aortic endothelial cell
HDL	High-density lipoprotein
HEK-293	Human embryonic kidney-293
HP	Hydrolysis product
IDL	Intermediate-density lipoprotein
OxLDL	Oxidized low-density lipoprotein

LDL	Low-density lipoprotein
LDLR	Low-density lipoprotein receptor
LOX-1	Lectin-like oxLDL receptor
Lp	Lipoprotein
LPL	Lipoprotein lipase
LRP	LDL receptor-related protein
M-CSF	Macrophage colony-stimulating factor
MDA	Malondialdehyde
mRNA	Messenger RNA
NADPH	Nicotinamide adenine dinucleotide phosphate
NEFA	Non-esterified free fatty acid
NOX	NADPH oxidase
NOXi	NADPH oxidase inhibitor
Nrf2	Nuclear factor-erythroid factor 2
PBS	Phosphate-buffered saline
PI3K	Phosphoinositide 3-kinase
PMA	Phorbol 12-myristate-13-acetate
PSGL-1	P-selectin glycoprotein ligand-1
PUFA	Polyunsaturated fatty acid
RNA	Ribonucleic acid
ROS	Reactive oxygen species
RPMI	Roswell Park Memorial Institute
rRNA	Ribosomal ribonucleic acid
SDS-PAGE	Sodium dodecyl sulfide polyacrylamide gel electrophoresis
SMC	Smooth muscle cell
snoRNA	Small nucleolar RNA
SOD	Superoxide dismutase

SRA	Scavenger receptor-A
SR-B1	Scavenger receptor class-B type 1
TBARS	Thiobarbituric acid reactive substance
TBHP	Tert-butyl hydroperoxide
TBST	Tris-buffered saline with Tween-20
TGRL	Triglyceride-rich lipoprotein
THL	Tetrahydrolypstatin
TNF-α	Tumor necrosis factor
VLDL	Very low-density lipoprotein

CHAPTER 1: INTRODUCTION

1. Background

1.1 Development and progression of atherosclerosis

Cardiovascular disease (CVD) is the second leading cause of death in Canadian adults, with about one in 12 (or 2.6 million) Canadian adults aged 20 and over living with diagnosed CVD (1). Atherosclerosis, which is defined by a thickening of the arterial intima caused by an accumulation of inflammatory cells, fibrous materials, and lipids that form plaque deposits during endothelial cell damage and constriction of the arteries, plays a significant role in vascular disorders (2). Studies on the disease have revealed cellular and molecular interactions in the arteries that lead to a specific sequence of changes in the vessel during atherogenesis, where smooth muscle cells (SMCs) and macrophages play important roles (3). Endothelial activation and dysfunction, caused by several factors, including oxidative and metabolic stress, during atherogenesis results in the recruitment of inflammatory cells, which include monocytes. The monocytes then undergo the process of macrophage differentiation and foam cell formation as a result of increased uptake and accumulation of oxidatively damaged low-density lipoprotein (LDL) (4). Foam cells are involved in complex molecular and cellular mechanisms, such as cholesterol uptake, efflux and esterification (5), that have been the subject of extensive research aimed at understanding atherosclerosis processes.

Endothelial cell (EC)-bound lipoprotein lipase (LPL) hydrolyzes triglyceride-rich lipoproteins (Lp). LDL enters the intima through the endothelial cells via transcytosis aided by proinflammatory cytokines. Initial lesion formation starts in the intima, where LDL changes due

to processes including reactive oxygen species (ROS) oxidation, which draws in monocytes. The monocytes develop into macrophages, and these macrophages, with increased scavenger receptor-A (SRA) and cluster of differentiation 36 (CD36) expression, internalize modified LDL to create foam cells (6). Prior studies have shown that macrophage foam cells play an important role in plaque instability, but recently, SMCs have been observed as a major source of foam cells in human and murine atherosclerosis in both early and advanced lesions (2,3,4). Macrophage or SMC-derived foam cells disrupt efferocytosis, phagocytic removal of dead or dying cells, and trigger several pathways of programmed cell death, including apoptosis, which leads to plaque instability as a result of enlarged necrotic cores due to the accumulation of dead cells in the atherosclerotic plaques (3). Thus, SMC-derived foam cells play an important role in the development of atherosclerosis.

Lesion initiation takes precedence during the early stage of atherosclerosis. The endothelium of blood vessels serves as a barrier between blood and tissue. Lesion formation usually takes place in regions of arterial branching or curvature where the blood flow is altered, and it results in increased permeability to macromolecules such as LDL (10). This increase in permeability results in a build-up of LDL in the sub-endothelial matrix. The ionic interactions between the positively charged lysine and arginine of the apolipoprotein B (apoB) constituent of LDL and the negatively charged sulfur matrix of proteoglycans in the intima (3) contribute to LDL retainment in the vessel wall for lesion formation. The retention of LDL in the vessel wall is aided by interactions between the LDL constituent apolipoprotein B (apoB) and matrix proteoglycans in the intima (11). Once in the intima, LDL is subjected to oxidation, proteolysis, lipolysis, and aggregation, and these modified LDL are taken up by macrophages which are

converted into foam cells (12). The modification of LDL leads to inflammation and foam cell formation, resulting in early lesion formation.

Atherosclerosis progresses due to excess circulating plasma LDL invading the sub-endothelial space, where the LDL is susceptible to oxidation, as seen in Figure 1 (7, 8). Oxidized LDL (oxLDL) promotes the adhesion of recruited monocytes to the endothelium and the migration of adherent monocytes into the sub-endothelial space, where they differentiate into macrophages that can take up the oxLDL (8). The continuing uptake of oxLDL results in dysregulated lipid metabolism in the macrophages and lipid accumulation that is more than the homeostatic capacity of the macrophages, which triggers the formation of lipid-laden foam cells. A fatty streak is formed (8,9) as a result of the accumulation of foam cells.

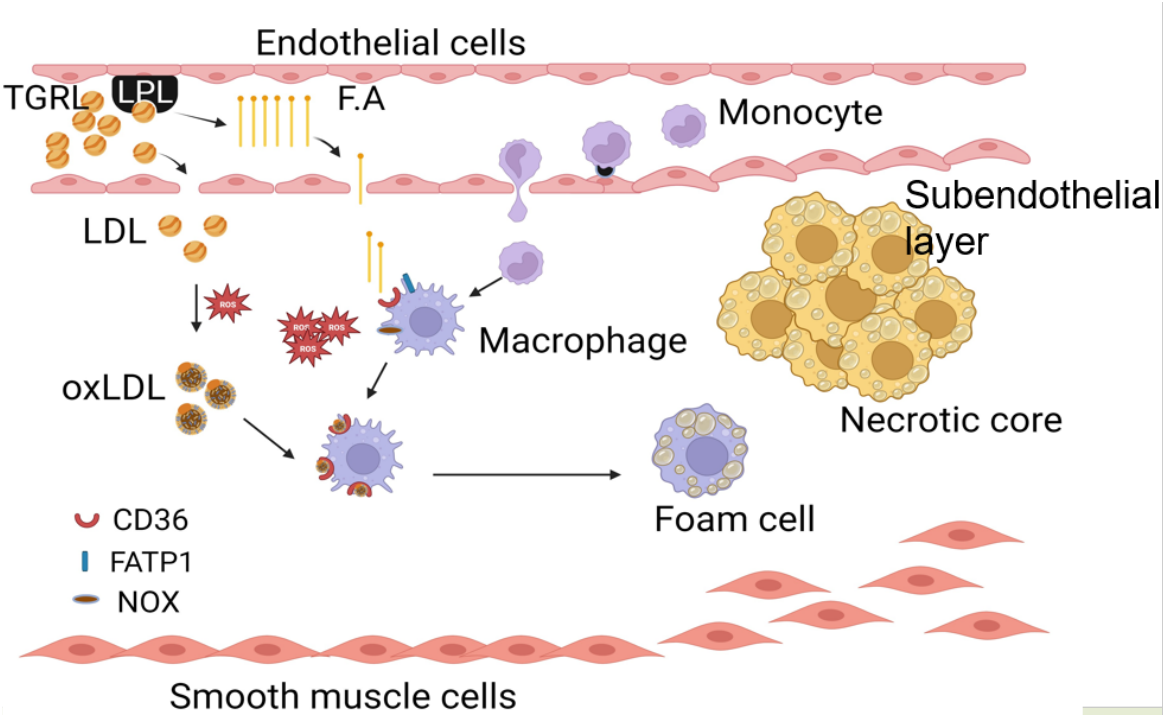

Figure 1: An overview of the development and progression of atherosclerosis.

Endothelial cell-bound LPL hydrolyzes triglyceride-rich lipoproteins (TGRL), like the very low-density lipoprotein (VLDL) in the plasma. Fatty acids and LDL are produced as a result of the hydrolyzed lipoproteins losing their lipid component and shrinking in size. Upon entering the sub-endothelial region, this lipoprotein undergoes oxidation, which causes monocyte chemotaxis. The monocytes differentiate into macrophages with the expression of NADPH oxidase (NOX) that produces more ROS, CD36, and fatty acid transport protein 1 (FATP1) and absorb oxLDL within the sub-endothelial layer, resulting in macrophage-derived foam cells. The smooth muscle cells take up oxLDL and produce foam cells in the intima. Lipid buildup causes a complicated, inflammatory reaction that forms a necrotic core and eventually results in plaque rupture. Figure created with BioRender (www.biorender.com).

During the initial lipid oxidation due to the production of ROS by the vascular cells, some minimally oxidized pro-inflammatory LDLs are formed. These minimally oxidized LDLs (mmLDL) possess pro-inflammatory activity and do not bind to the scavenger receptors of macrophages but rather retain their affinity for Low-density lipoprotein receptor (LDLr) for mmLDL's uptake (6). The mmLDL upregulates the expression of scavenger receptors for oxLDL binding, which causes an increase in pro-inflammatory molecule expression. Minimally oxidized LDL engages Toll-like receptor 4 and activates the NF-κB pathway, leading to the activation of pro-inflammatory signaling cascades. The proinflammatory cascade includes leukocyte chemotaxis, platelet aggregation, and foam cell formation induced by the activated lectin-like oxLDL receptor (LOX-1) in the vascular cells.

The progression of the early stage of atherosclerosis is characterized by an increase in pro-inflammatory molecule expression. The pro-inflammatory molecules with enhanced expression include P-selectins, E-selectins, cell adhesion molecules, and growth factors like macrophage colony-stimulating factor (M-CSF) in the intima of the artery. These adhesion molecules and chemotactic factors have complementary carbohydrate ligands, like P-selectin glycoprotein ligand-1 (PSGL-1), to E-selectins, which are present in monocytes (6, 13, and 14). Thus, the enhanced expression of adhesion molecules and chemotactic factors results in the recruitment of monocytes at the lesion site in the intima.

The proliferation and differentiation of monocytes into macrophages inside the intimal layer are stimulated by M-CSF. M-CSF contributes to function changes in the macrophages, including increased scavenger receptor expression. The differentiated macrophages can internalize highly oxidized LDL particles rapidly, and the minimally oxidized LDLs are internalized slowly via LDLr regulation (15). ROS, which are assumed to be produced by ECs,

macrophages, and enzymes in human atherosclerotic lesions, are thought to be involved in this change of mildly oxidized to highly oxidized oxLDL particles (6). M-CSF is therefore essential for the development and differentiation of monocytes into macrophages, as well as for the uptake of oxLDL by macrophages.

Several receptors that recognize a wide range of ligands and are responsible for the internalization of oxLDL in the macrophages are called scavenger receptors. SR-A and CD36 are the major scavenger receptors (17), whose expression is controlled by the cytokines tumor necrosis factor-α (TNF-α) and interferon-γ, and the transcription factor peroxisome proliferator-activated receptor-γ (18). These receptors aid in enhancing the uptake of oxLDL particles by macrophages, contributing to foam cell formation.

As atherosclerosis progresses, another major phenomenon seen is the proliferation and migration of SMC, which are stimulated by cytokines and growth factors released by macrophages and T cells. These SMCs take up oxLDL and change into foam cells in a manner similar to macrophages. OxLDL activates the SMCs, which then produce a number of extracellular matrix proteins that lead to the production of fatty streaks and a fibrous cap by the foam cells (19, 20, 21). Once the foam cells interact with the cytokines in the sub-endothelial region, the foam cells begin to die. This causes the release of their lipid-filled contents and extracellular cholesterol as well as the creation of the necrotic core, which is a feature of advanced atherosclerotic plaques (19, 20). Certain fatty streaks in the intima include an aggregation of migratory SMCs. Furthermore, the SMCs secrete fibrous substances that result in occlusive fibrous plaques that enlarge over time. A growing quantity of extracellular lipids, primarily cholesterol and cholesteryl esters, as well as the accumulation of SMCs and extracellular matrix generated from SMCs, are characteristics of fibrous plaques (6). As a result,

the creation of the plaque involves SMCs, foam cells, and the extracellular matrix. Advanced atherosclerotic plaques constrict the artery lumen *in vivo*, which mostly causes the ischemic symptoms of atherosclerosis. Nonetheless, neovascularization acts to weaken the atherosclerotic plaque along with the matrix metalloproteinases released by macrophages and smooth muscle cells (22, 23). Vulnerable plaques are characterized by thin fibrous caps and an increase in inflammatory cells. Maintaining a balance between matrix formation and breakdown is essential for maintaining the fibrous cap, and inflammatory cell secretions are likely a mediator of both processes. Plaque rupture is, therefore, more likely in lesions with a big necrotic core and a thin fibrous cap. This causes the vessel to thrombose, which may ultimately result in an acute cardiovascular event like a stroke or myocardial infarction (24, 25). The atherosclerotic plaques' composition and susceptibility to rupture play a critical role in the development of thrombus formation.

1.2 Lipids and lipoproteins

1.2.1 Lipids

Lipids and their building blocks, free fatty acids, perform critical cellular functions. Lipids are an inherent component of the cell membrane that demarcate the boundaries of the cell and intracellular organelles (26). Lipids can also act as signaling molecules that regulate physiological processes.

In the cell membrane, numerous classes of lipids interact with proteins to perform crucial structural tasks, serve as signaling molecules, and supply energy to cells through oxidation.

Lipids can serve as energy reserves in the body and are easily accessible to the cells when energy is needed, allowing the body to go for up to several weeks without consuming any food. An essential part of the cell membrane is the phospholipids. Typically, the structure consists of a glycerol backbone, two hydrophobic fatty acyl tails, and a hydrophilic phosphate group. Phospholipids are, thus, amphipathic. The bilayer arrangement of phospholipids in the cell membrane acts as a barrier that prevents some molecules from entering the cells and also protects the cells. The hydrophobic portion of the phospholipid bilayer faces in, while the hydrophilic portion faces out. This bilayer configuration helps in regulating which molecules can enter and leave the cell. Small non-polar molecules, like oxygen, and polar molecules, like water, can easily diffuse into and out of the cell. Transport proteins are necessary for the easy passage of large, polar molecules like glucose (27). Sterols, which have a structure of four fused rings, are a different class of lipid. Cholesterol is an important type of sterol. Cholesterol is the precursor to several steroid hormones, including testosterone, cortisol, and estrogen, and it is synthesized in the liver. Cholesterol also exists in cell membranes, where it enters the bilayer and affects the fluidity of the membrane (27). Even though cholesterol is necessary for the structural integrity of cells, the pathological buildup of cholesterol in arterial walls causes atherosclerosis and cardiovascular disease.

1.2.2 Lipoproteins

Lipoproteins, a complex assembly of lipids and proteins, carry lipids such as triglycerides and cholesterol through the blood to different tissues. Lipoproteins play an important role in several biological processes (28), which include transport of dietary lipids from the gut, transport lipids from the liver to peripheral tissues throughout the body, and reverse cholesterol transport.

The structure of a lipoprotein consists of a central hydrophobic core of non-polar lipids of predominantly cholesteryl esters and triglycerides. A hydrophilic monolayer made of phospholipids, free cholesterol, and apolipoproteins encircles this hydrophobic core (29) (Figure 2). Based on their size, density, lipid composition, and apolipoprotein composition, plasma lipoproteins are classified into four major types: chylomicrons, very low-density lipoproteins, low-density lipoproteins, and high-density lipoproteins (Table 1).

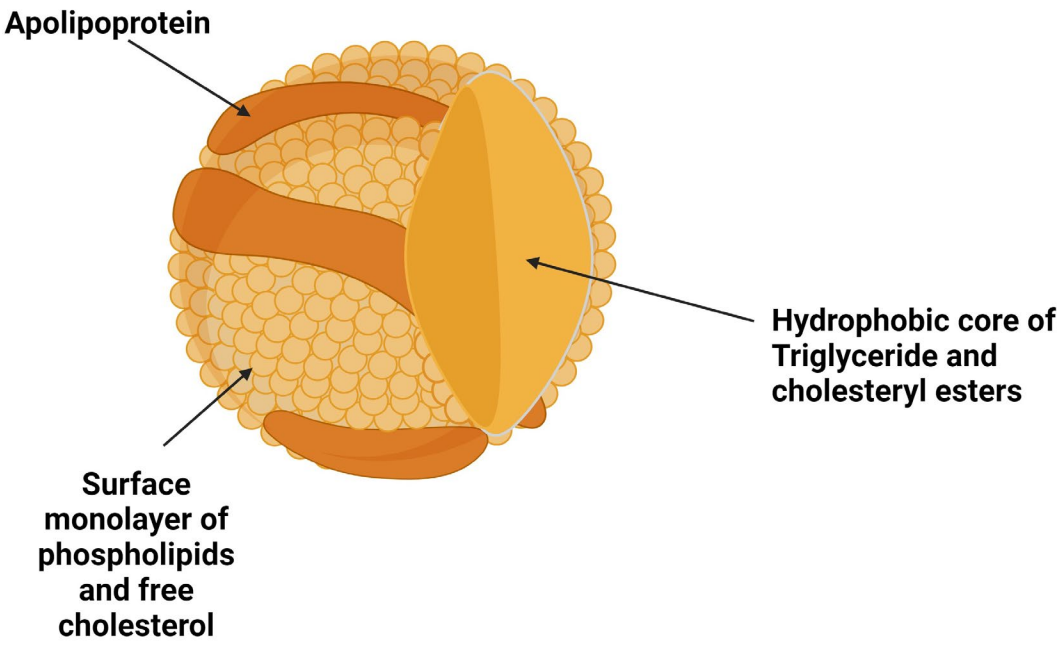

Figure 2: Structure of lipoproteins.

Lipids are transported through the bloodstream by the protein-lipid complexes known as lipoproteins. Triglycerides and cholesteryl esters, which are mainly non-polar lipids, need to be enclosed in a phospholipid monolayer for lipid transport to occur. The membrane is made up of phospholipids with the polar head groups facing outward and the non-polar tails pointing inward. Proteins and unesterified cholesterol can also be found on the lipoprotein membranes. Figure created with BioRender (www.biorender.com).

Table 1: Major classes of lipoproteins.

Properties	**Chylomicron**	**VLDL**	**LDL**	**HDL**
Source:	Gastrointestinal tract	Liver	Liver	Liver and small intestine
Density (g/mL):	< 0.94	0.96 – 1.006	1.019 – 1.063	> 1.064 – 1.21
Diameter (nm):	75 -1200	30 -80	22 -27.5	7 - 14
Apolipoprotein composition:	apo A-I, A-II, A-IV, A-V, B-48, C-II, C-III, and E	apo B-100, C-I, C-II, C-III, and E	apo B-100	apo A-I, A-II, A-IV, C-I, C-II, C-III, and E
Major structural protein:	apo B-48	apo B-100	apo B-100	apo A-I
Major lipid component:	Triglyceride Phospholipid	Triglyceride Phospholipid	Cholesterol Phospholipid	Cholesterol, Phospholipid

Note. Source of information on lipoprotein characteristics (29).

1.2.3 Lipoprotein receptors and lipid transporters

Several receptors and transporters play important roles in lipoprotein metabolism. Major receptors and transporters involved include the LDL receptor; LDL receptor-related protein 1; scavenger receptor B-1; ATP-binding cassette transporters A1, G1, G5, and G8; and Niemann-Pick C1-like 1 (Table 2).

Table 2: Lipoprotein receptors and lipid transporters.

Receptors or transporters	**Functions**
LDL Receptor	Facilitates the uptake of LDL, chylomicron remnants, and Intermediate-density lipoprotein (IDL) through endocytosis. apo B-100 and apo E recognition.
LDL Receptor Related Protein 1 (LRP1)	Uptake of VLDL and chylomicron remnants and contributes to the clearance of circulating apo E.
ATP-Binding Cassette Transporter A1 (ABCA1)	Facilitates the transfer of phospholipids and cholesterol from the cell to pre-beta-1 HDL particles with low lipid content.
Scavenger Receptor B1 (SR-B1)	Facilitates the selective uptake of cholesteryl esters from HDL particles in the liver and steroid-producing cells. It enables the outflow of cholesterol from the cell to HDL particles in macrophages and other cells

ATP-Binding Cassette Transporter G1 (ABCG1)	Mediates the outflow of cholesterol from the cell to HDL particles.
ATP-Binding Cassette Transporter G5 and G8 (ABCG5/ABCG8)	Mediates the transfer of cholesterol and plant sterols from the inside of enterocytes into the intestinal lumen, reducing their absorption and preventing the absorption of dietary plant sterols. Carries bile and plant sterols from the liver into the bloodstream, aiding in the excretion of plant sterols.
Niemann-Pick C1-Like 1 (NPC1L1)	Facilitates the uptake of cholesterol and plant sterols into the enterocyte from the intestinal lumen

Note. Several receptors and transporters play important physiological functions in lipoprotein metabolism (29 - 37).

1.2.4 Lipoprotein lipase

LPL is an extracellular lipase on the vascular endothelial surface that belongs to the *sn*-1 lipase family, which hydrolyzes specifically the ester bonds at the *sn*-1 and *sn*-3 positions of triglycerides. LPL hydrolyzes the triglycerides transported in CMs and VLDL to liberate fatty acids for use by cells. The catabolized triglycerides lead to the conversion of CMs and VLDL into smaller 'remnant' lipoproteins. LPL also functions as a molecular bridge, bringing plasma lipoproteins very near to cell surface receptors to aid lipoprotein uptake into cells (38). Thus, LPL possesses both catalytic and non-catalytic roles in Lp metabolism. LPL has been demonstrated to be expressed in muscle, heart, macrophages, and adipose tissue and secreted by

exocytosis (39). LPL is usually associated with the cell surface protein (39), glycosyl phosphatidyl inositol-anchored high-density lipoprotein binding protein, and with the cell surface by binding to heparan sulfate proteoglycan receptor after secretion.

Understanding the role of LPL is important in understanding the biology of atherosclerosis and its clinical manifestations (40). LPL consists of an N- and a C-terminal connected by a hinge region. The N-terminal α/β-hydrolase domain contains six α-helices and 10 β-strands bearing the catalytic triad (S159, D183, and H268), while the C-terminal flattened β-barrel domain contains 12 β-strands. The LPL's lid region, a loop extending from the C243–C266 disulfide bond that can undergo conformational changes creating an interfacial activation of the LPL active site, was revealed to be an open conformation. The crystallized structure of LPL revealed two N-linked glycans, five disulfide bonds, an active site cleft that is lined by the hydrophobic side chains, which form van der Waals interactions (41) and stabilizes the hydrophobic tails of lipid substrates in the active site, and a calcium atom harbored by A194, R197, S199, D201, and D202.

Triglycerides are hydrolyzed into fatty acids and monoglyceride by LPL. Triglyceride-derived fatty acids are subsequently used as fuel for skeletal or cardiac muscle or as a reserve in adipose tissue. Apo-CII, a cofactor for LPL that is usually transported by a chylomicron along with VLDL and IDL, is necessary for LPL activation. By eliminating the fatty acids from triglycerides, LPL shrinks the chylomicrons, which are then taken up by the liver via receptor-mediated endocytosis. The fatty acids hydrolyzed from the triglycerides may be stored in adipocytes or used as an energy source in skeletal and cardiac muscle (40).

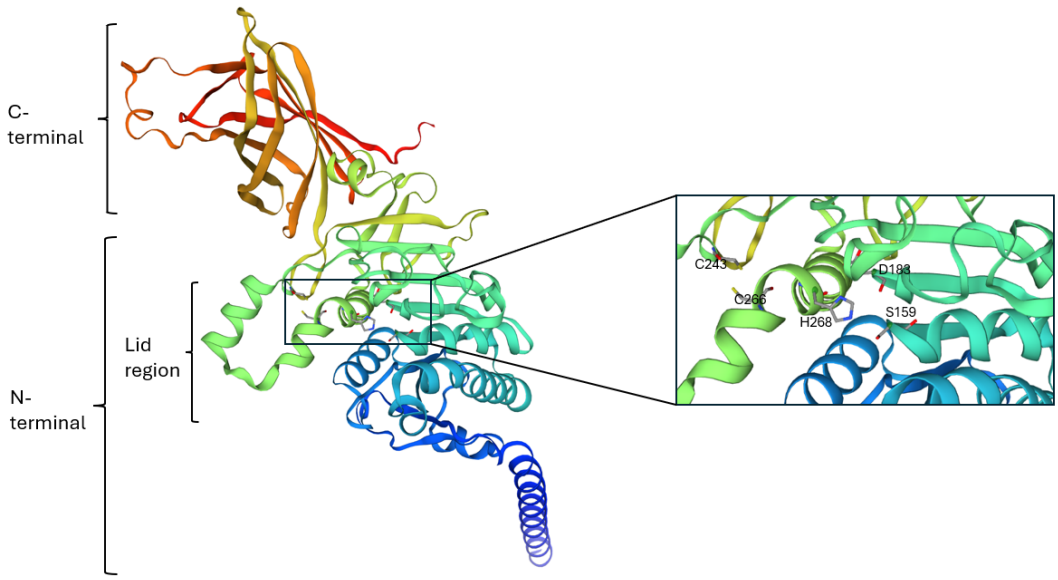

Figure 3: Structure of lipoprotein lipase.

A modeled structure of the LPL, depicted by cartoon representation, contains an N-terminal made up of 6 α-helices and 10 β-strands and a C-terminal made up of 12 β-strands. The C243 – C266 of the lid region is seen to be in close proximity to the catalytic triad of the active site. Figure created with Swiss model (www.swissmodel.expasy.org) and PowerPoint.

Hereditary dyslipidemias (particularly type one) or hyperchylomicronemia clearly show the pathophysiology of LPL. A substantial increase in triglyceride levels, >1000 mg/dL, characterizes the genetically inherited condition known as hyperchylomicronemia, which causes the plasma of affected individuals to appear milky (40). Furthermore, these people have much higher chylomicron levels in their blood.

LPL is clinically significant in the development of atherosclerosis. According to a previous study, the free fatty acids (FFA) that LPL released from VLDL showed enhanced lipid droplet deposition in human THP-1 monocytes (16). This suggests that LPL may contribute to the macrophages' conversion to foam cells when LDL and oxLDL are collected by macrophages expressing LPL in the location of atherosclerosis. Furthermore, higher LPL mass and activity in post-heparin plasma were discovered in patients with advanced atherosclerosis (42). LPL aids in the production of atherogenic lipoproteins. Chylomicrons and VLDL are affected by LPL, which hydrolyzes the triglycerides they contain, to yield chylomicron remnants and VLDL remnants. With a high concentration of cholesteryl esters, the remnant lipoproteins are then internalized into macrophages through receptor-mediated endocytosis (43). LPL released free fatty acids, which macrophages re-esterify. This causes a buildup of cholesteryl esters in macrophages, which causes macrophages to change into foam cells. Following the conversion of VLDL to IDL by LPL, another *sn*-1 lipase, catalyzes the hydrolysis of triglycerides and phospholipids on IDL to make the smaller, denser LDL. Additionally, foam cells are produced when macrophages incorporate oxLDL via the vascular endothelium using their scavenger receptor (40). These foam cells are crucial in the formation of plaque and aid in the development of atherosclerosis. Increases in TNF-α release, adhesion molecule expression, and activation of oxidative stress

have all been linked to increased lipolysis of triglyceride-rich lipoproteins near the endothelium, which increases endothelial layer permeability (2).

1.2.5 Lipoprotein metabolism

Triglycerides and cholesterol, which are hydrophobic lipids, are transported within the interstitial fluid and plasma by lipoprotein metabolism. It involves the transport of cholesterol from the liver and intestine to peripheral tissues and reverse transport to the liver, and also the transport of triglycerides from the intestine and liver to the muscles for energy and adipose tissue.

Dietary lipids and cholesterol are absorbed by intestinal enterocytes in the exogenous pathway of lipid transport (Figure 4), and integrated into chylomicrons, which contain the primary structural protein called the apoB-48. Chylomicrons are initially released into the lymph, avoiding the hepatic first-pass impact. Chylomicrons bind to LPL on the luminal surface of the capillary endothelium of tissues, especially that of the muscle and adipose tissue, after they enter systemic circulation (43). Triglycerides are hydrolyzed by LPL (with apoC-II on the surface of chylomicrons being a necessary cofactor for LPL). The triglyceride-depleted chylomicron remnant is liberated as the free fatty acids enter the tissue, where they will be utilized for energy in muscle or stored, as in adipose.

The liver produces triglycerides and cholesteryl esters and packages them into VLDL, which contain the main structural protein apoB-100, as part of the endogenous mechanism of lipid transport (Figure 5). LPL hydrolyzes triglycerides within the released VLDL, which results in the formation of IDL. The apo E contained in the IDL formed has affinity for the LDL

receptor and also the LRP and allows IDL to be taken up by the liver. Alternately, Hepatic lipase (HL) in the hepatic sinusoids can hydrolyze the triglyceride and phospholipid in IDL to form LDL. Through the interaction of Apo B-100 with the LDL receptor, LDL formed can be absorbed by the liver or by peripheral cells (43).

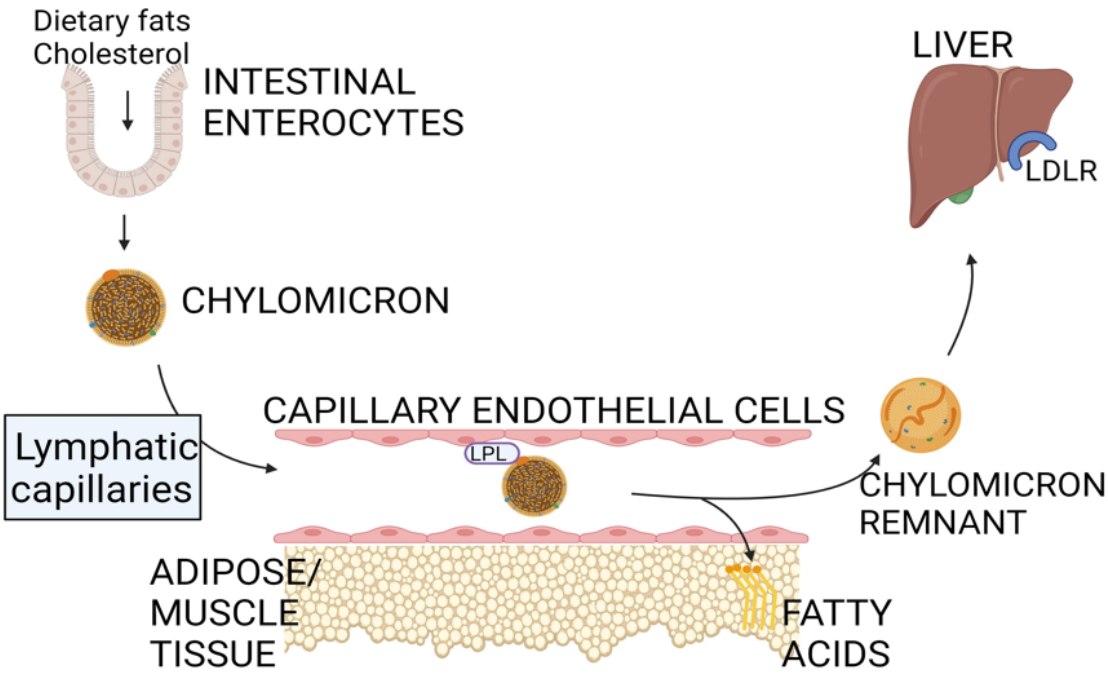

Figure 4: Exogenous pathway of the lipid transport.

Dietary fats and cholesterol are packed into chylomicrons in the gut. When these triglyceride-rich lipoproteins enter the bloodstream via the lymphatic capillaries, LPL preferentially hydrolyzes their triglycerides to produce chylomicron remnants and FFA, which are then used by the tissues. Chylomicron remnants, a smaller and denser form of chylomicron, are produced as a result of the hydrolysis of triglyceride and phospholipid. The LDLR in the liver takes up the chylomicron remnants from the bloodstream and uses them for a variety of physiological functions, such as the synthesis of VLDL. Created with BioRender (www.biorender.com).

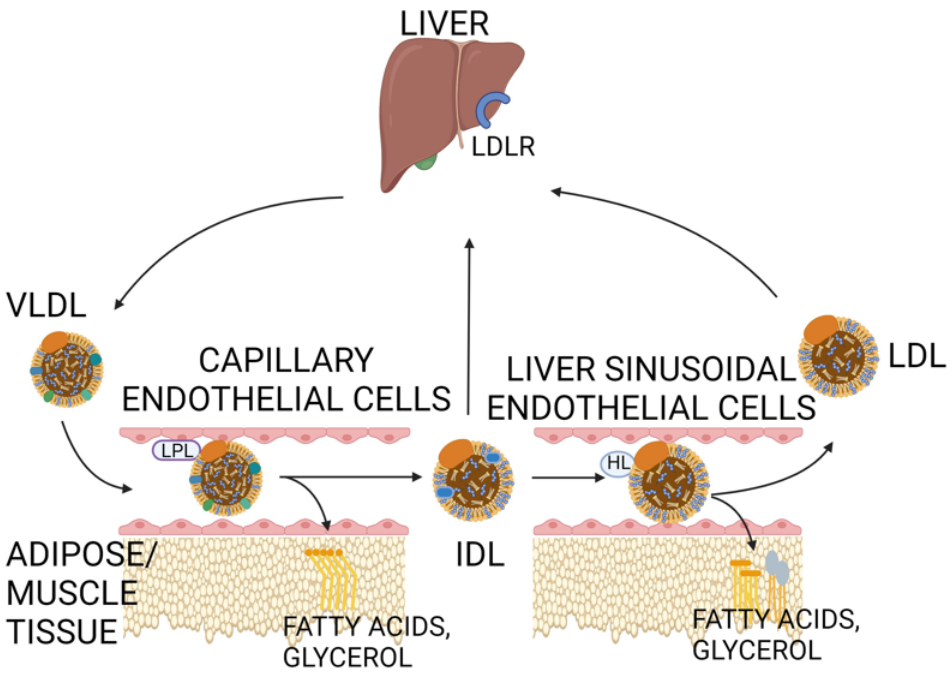

Figure 5: Endogenous pathway of lipoprotein metabolism.

VLDL released into the bloodstream by the liver is metabolized into denser and smaller IDL. HL further hydrolyzes the IDL in the bloodstream to release FFAs. IDL hydrolysis by HL leads to the loss of triglycerides and phospholipids molecules in IDL to form cholesterol-enriched LDL. Tissues utilize the cholesterol molecules in LDL for various physiological functions. The liver further removes LDL from the bloodstream via LDLR receptor-mediated endocytosis. Created with BioRender (www.biorender.com).

Complex mechanisms govern reverse cholesterol transport and HDL metabolism. The gut and the liver both produce HDL and its main apolipoprotein, apoA-I. Only the liver produces apoA-II, a second important HDL protein. The cellular protein ABCA1 promotes the interaction of nascent HDL, the initial form of HDL particle present in the early stages of reverse cholesterol transport, with peripheral cells to assist in the elimination of surplus free cholesterol. Lecithin-cholesterol acyltransferase (LCAT) transforms some of the acquired free cholesterol into cholesteryl ester on the HDL particle, resulting in the development of the bigger HDL_3 particle. By continued activity of the LCAT, HDL gains additional cholesteryl esters and finally develops into the bulkier HDL_2. Utilizing the SR-BI HDL receptor in the liver, HDL_2 can selectively transport both free and cholesteryl ester cholesterol to the liver. The cholesteryl ester transfer protein can also transfer cholesteryl esters from HDL_2 to apoB-containing lipoproteins such as VLDL and LDL (43). The cholesteryl esters are subsequently recycled back into the liver by the hepatic uptake of LDL. Endothelial lipase (EL) and HL can hydrolyze HDL_2 triglycerides and phospholipids to transform them into HDL_3. The cholesterol from HDL is finally eliminated as bile acid or free cholesterol in the bile and feces. HDL cholesterol contributes to the hepatic cholesterol pool required for bile acid production. The reverse cholesterol transport process is summarized in figure 6.

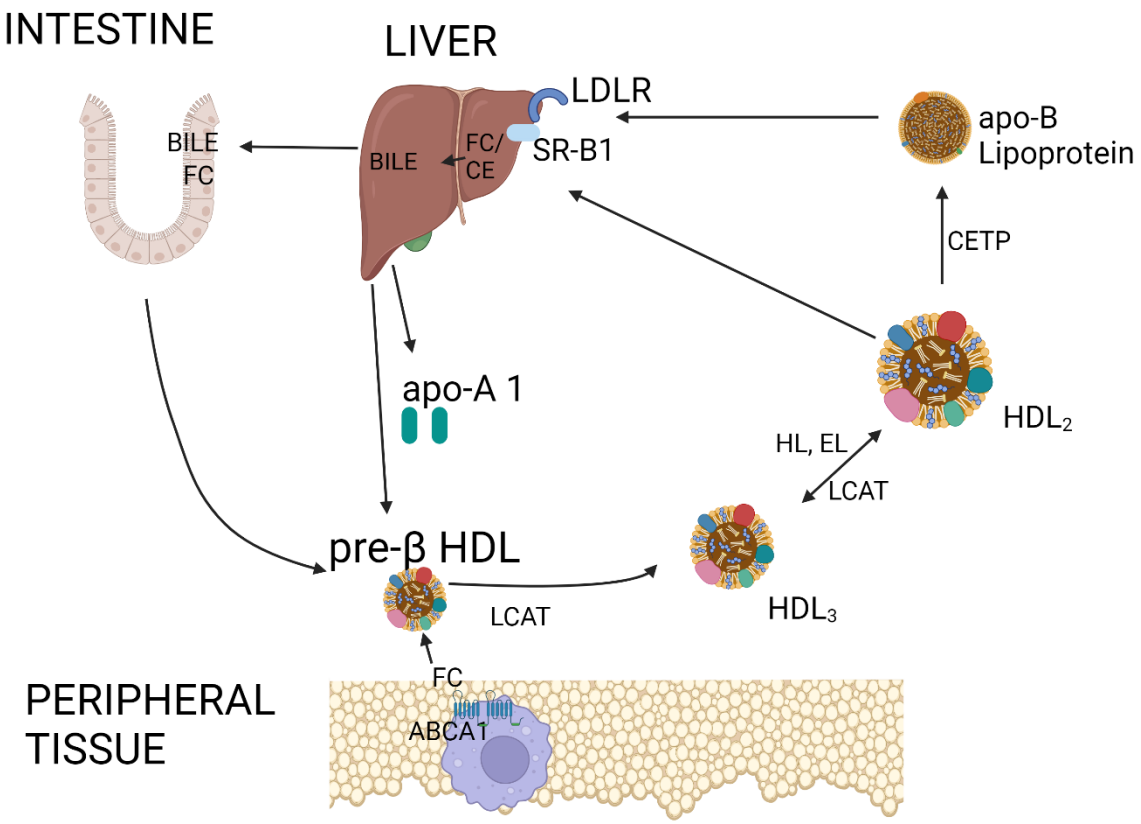

Figure 6: Reverse cholesterol transport

Excess cholesterol present in peripheral tissues is eliminated via reverse cholesterol transport and HDL metabolism. The nascent HDL, pre-β-HDL, is formed by apoA-I acquiring free cholesterol and phospholipid via ABCA1 from peripheral cells. LCAT esterifies some of the acquired free cholesterol into cholesteryl ester on the HDL particle. With the aid of the SR-BI, both free cholesterol and cholesteryl esters can be selectively taken up to the liver. The cholesteryl ester transfer protein (CETP) aids the transfer of cholesteryl esters from HDL_2 to VLDL and LDL, and the cholesteryl esters are subsequently recycled back into the liver by the hepatic uptake of LDL via the LDLr. EL and HL can hydrolyze HDL_2 triglycerides and phospholipids to transform them into the smaller HDL_3. The cholesterol is eliminated as bile acid or free cholesterol. Created with BioRender (www.biorender.com).

1.3 Hydrolysis products of lipoprotein lipases

Free fatty acids and monoglycerides are liberated from the triglyceride component of lipoprotein through hydrolysis by LPL. Fatty acids are used by the cell as fuel when it needs a lot of energy or during starvation. Fatty acids, with the exception of steroids, are carboxylic acids that provide the structural basis for fats, oils, and all other types of lipids. Fatty acids are typically unbranched, contain an even number of carbon atoms (often 4–28), and can be divided into groups based on the quantity and presence of carbon-carbon double bonds. Saturated fatty acids contain no carbon-to-carbon double bonds, while monounsaturated fatty acids have one, and polyunsaturated fatty acids have two or more carbon-to-carbon double bonds. In *trans* fatty acids, the hydrogen atom attached to each carbon comprising a double bond are on the opposing sides of the fatty acid structure, while *cis* fatty acids have hydrogen atoms on the same side (44).

The efficient transport and metabolism of cholesterol depend on the presence of essential fatty acids, linoleic and alpha-linolenic acids, as well (44). Excess lipid buildup in cells is caused by the cells' imbalanced acquisition and utilization of fatty acids. Foam cells, which are connected to atherosclerosis, are produced when excessive amounts of lipids are accumulated in cells (45).

1.3.1 Fatty acids and atherosclerosis

It is important to study how fatty acids and their lipid metabolites contribute to the onset and progression of inflammation and atherosclerosis. Fatty acids play both pro- and anti-atherogenic roles in atherogenesis, contributing in various ways. By taking part in numerous signaling pathways, they may contribute to inflammation and endothelial dysfunction (46).

Saturated fatty acids are believed to have pro-inflammatory effects that result from altering the plasma membrane structure of cells and through the direct stimulation of pro-inflammatory signaling pathways. Palmitic acid, a saturated fatty acid, can trigger inflammatory responses in macrophages by increasing the production of pro-inflammatory cytokines like TNF-α and IL-6 and the transcriptional activity of nuclear factor kappa B (NF-κB) (90). Palmitic acid can also promotes the pro-inflammatory M1 phenotype in macrophage polarization (90). In addition, polyunsaturated fatty acids (PUFAs) have a more complex effect on inflammation. PUFAs can affect the stability of lipid rafts and the fluidity of plasma membranes, and they can serve as a substrate for the synthesis of lipid mediators that control inflammation.

An increasing amount of research indicates that PUFAs contribute differently to inflammation (47, 49). Arachidonic acid, which belongs to the omega-6 PUFAs, is a substrate for the biosynthesis of prostaglandins and leukotrienes, which are involved in the onset of inflammation (48). However, lipoxin A4, which is thought to have a significant role in the reduction of inflammation, can be biosynthesized using arachidonic acid (49). Clinical trials are being conducted to uncover new medications that have a good impact on lipid metabolism and atherogenesis (50), and these studies are focused on the anti-inflammatory characteristics of Ω-3 PUFAs.

Fatty acids play a variety of roles in the functioning of several vascular wall cells, including endothelial cells, which buttresses their involvement in atherogenesis. All blood vessels, including arteries, capillaries, and veins, are lined by endothelial cells, which act as a barrier to ensure optimal blood flow (51). The AMPK/PI3K/Akt/eNOS signaling pathway is downregulated by palmitic acid in both *in vivo* (mouse) and *in vitro* (cardiac microvascular endothelial cell) models, which may contribute to endothelial dysfunction (46). Inflammation

brought on by a high-fat diet in mice may increase endothelial permeability (52). Plasma markers, inter-cellular adhesion molecule-1 (ICAM-1) and vascular cell adhesion molecule-1(VCAM-1), of endothelial activation were upregulated in response to elevated levels of plasma triglycerides in healthy male subjects infused with 20% fat emulsion (53). It was discovered that palmitate increases the expression of the interleukins (IL)-6, IL-8, Toll-like receptor 2, and ICAM-1 in an experiment with human adipose microvascular endothelial cells (54). ICAM-1 surface expression caused by palmitate facilitated monocyte binding and transmigration.

Fatty acids have been seen to play important roles in activating oxidative stress. Excessive FFA exposure in atherosclerotic macrophages results in impaired signaling pathways, such as the PI3K/Akt signaling pathway, NF-κB signaling pathway, PPAR-ɣ signaling pathway, and apoptosis signaling pathway (91), induces macrophage apoptosis, impairs efferocytosis (92), and induces oxidative stress (92). A previous study noted the impact of linoleic acid and the pancreatic beta-cell activity of the fatty acid receptor GPR40 on the assembly and activation of NOX, an enzyme that catalyzes ROS generation (55). Superoxide and hydrogen peroxide concentrations, in the presence of 5.6 and 8.3 mM of glucose, were both raised by linoleic acid in pancreatic β-cells. Additionally, activation of GPR40 resulted in the translocation of p47phox to the plasma membrane at 5.6 mM of glucose but not at 16.7 mM of glucose. The rise in superoxide in the presence of linoleic acid was eliminated by p22phox knockdown. A prior study in 2020 revealed that acute activation of a fatty acid receptor results in pancreatic cell NOX activation and an increase in ROS production (55).

1.4 Reactive oxygen species production and oxidative stress in atherosclerosis

Excess lipid buildup has been characterized by ER membrane remodeling and mitochondrial dysfunction, which activates the cell's oxidative stress response, producing ROS (56). Oxidative stress, activation of pro-inflammatory signaling pathways, and stimulation of cytokine release, usually occur simultaneously and are well-known aspects of the pathophysiology observed early in atherosclerosis. According to several studies, the overproduction of ROS is essential to the emergence of CVD. Superoxide ($O_2^{\bullet -}$), hydrogen peroxide (H_2O_2), hydroxyl radicals ($HO^{\bullet}$), and singlet oxygen are some of the ROS that are produced when ambient or cellular oxygen is partially reduced (57). Since ROS are physiologically necessary to cells because they participate in cellular functions, signaling, and viability, it is crucial to maintain their basal levels. Superoxide is produced as a result of the reduction of molecular oxygen. As a result, superoxide can either be transformed into diatomic oxygen or hydrogen peroxide with the aid of the mitochondrial enzyme superoxide dismutase (SOD). Hydrogen peroxide, which is generally low-reactive without catalysts, produces hydroxyl radicals through the Fenton reaction (58). The hydroxyl radicals have harmful effects on molecules and biological structures.

In the cell, ROS are produced through a variety of enzymatic pathways, the majority of which start with the synthesis of superoxide and end with the generation of more reactive species. Superoxide can be synthesized as a byproduct of metabolism, even while enzymes like NOX purposely do so. These chemically reactive oxygen radicals exhibit their effects at the molecular level and range in reactivity. Increased ROS generates oxidative stress and plays a crucial role in the development of CVDs, despite the fact that they play beneficial roles in cells. Atherosclerotic lesions are formed as a result of various factors including oxidative stress (58).

The overproduction of ROS in atherosclerosis is caused by the migration of monocytes, T-lymphocytes, and mast cells within the arterial walls, which activates inflammatory processes and releases cytokines. For instance, a study found that the amount of the cytokine TNF-α increased proportionally to the quantity of mitochondrial ROS. Furthermore, NOX-mediated ROS production was boosted by other cytokines, such as interferon-ɣ and interleukin-1β (59). Macrophages generate ROS through several key mechanisms. The primary mechanism involves the production of ROS by various isoforms of NOX in different cell compartments, including the phagosomal membrane, resulting in an "oxidative burst" of ROS within the phagosome of the macrophages (94). This oxidative burst destroys ingested pathogens. Other ROS-generating mechanisms include ROS generated in the mitochondria (95), another critical site of ROS production in macrophages, and ROS produced as byproducts of cellular metabolisms (95, 96), like fatty acid oxidation.

1.5 NADPH oxidases (NOX)

NOX are enzymes responsible for converting molecular oxygen to superoxide, a ROS, where the NADPH component of the enzyme acts as the electron donor. The family of NOXs was first discovered in the membranes of phagocytic macrophage cells (60). There are seven identified members of the NOX family, which includes NOX1, NOX2, NOX3, NOX4, NOX5, and two large NOX5-like dual oxidases, DUOX1 and 2. All seven NOX isoforms are transmembrane protein complexes made up of six heteromeric subunits. Four of the enzyme subunits are located in the cytosol and are in the resting state, while the enzyme complex contains two integral membrane proteins. External stimuli, such as pathogen recognition or chemical activators, control how the subunits are put together and transported to the membrane,

where they interact and develop the capacity to produce superoxide anions by reducing oxygen. Superoxide produced by NOX-mediated macrophages serves as a potent primary microbicidal agent and is used as the first line of defense in innate immunity (61). Increased superoxide production by NOX is stimulated by lipid-induced activation of protein kinase C. In physiologically normal states, there is minimal NOX expression. However, it has been demonstrated that when the cells are exposed to mitogenic or transforming growth factors, excessive glucose levels, or hyperlipidemia, NOX expression rises significantly. These factors encourage the development of oxidative stress by increasing ROS production. The level of ROS production is determined by NOX expression. Phosphorylation-dependent mechanisms are involved in the activation of NOX. Phosphatidylinositol 3-phosphate (PIP), phosphatidylinositol 4,5-bisphosphate (PIP2), and phosphatidylinositol 3,4,5-trisphosphate (PIP3) are phosphatidylinositol derivatives generated by PI3K that binds with high specificity to the PX domain of p47phox (a regulatory subunit of NOX). This binding helps translocate p47phox, a cytosolic oxidase subunit, to the membrane, where it interacts with p22phox. p47phox-p22phox interaction is necessary for NOX, especially NOX2, activation (104). The presence of non-coding RNAs, DNA methylation, changes in the activity of transcriptional factors, control over mRNA stability, and post-translational modification of histones are all part of the epigenetic regulation of NOX production, according to studies (62,63,143). Therefore, numerous factors that control the level of ROS production in the body affect how NOX expression is regulated.

1.5.1 Structure and assembly of NOX

The term "NOX" refers to the first isoform of NOX2 to be characterized. It consists of six distinct subunits that work together to produce an active enzyme complex that generates

superoxide. The large heterodimeric component flavocytochrome b558 (cyt b558) is made up of two NOX subunits, gp91phox (the b subunit) and p22phox (the a subunit), which are integral membrane proteins. The multidomain regulatory subunits p40phox, p47phox, and p67phox coexist in the cytosol under resting conditions. After being stimulated, p47phox is phosphorylated. The whole complex then moves to the membrane where it joins with cyt b558 to create the active oxidase (64). The prosthetic group flavin and the electron-carrying heme group(s) are used by the activated complex to transfer electrons from the substrate to molecular oxygen. Rac2 and Rap1A, two low-molecular-weight guanine nucleotide-binding proteins, are also needed for the complex to be activated. Rap1A is a membrane protein, whereas Rac2 is localized in the cytoplasm in a dimeric complex with Rho-GDI (guanine nucleotide dissociation inhibitor). When Rac2 is activated, it binds guanosine triphosphate (GTP) and translocates to the membrane with the cytosolic complex of p40phox, p47phox, and p67phox.

The plasma membrane is internalized during phagocytosis and it eventually becomes the phagocytic vesicle's interior wall. The internalized target is then submerged in a toxic mixture of oxidants when superoxide is released into the vesicle via the enzyme complex and converted into its successor products. The fusion of secretory vesicles delivers rap1A and cyt b558 to the plasma membrane, enabling the release of these proteins to the environment. The identification of gp91phox homologs has considerably enhanced our understanding of free radical production and has shown that ROS production is not limited to phagocytic cells. These gp91phox homologs are collectively referred to as the NOX family (65), which contains a number of members with differential expression, including NOX1, NOX2, NOX3, NOX4, NOX5, and dual oxidase Duox proteins (Duox1 and Duox2).

Some members of the NOX family have extra characteristics, such as an extra N-terminal transmembrane domain or a peroxide homology domain. Six transmembrane domains make up NOX2, also known as gp91phox, and both the C- and N-termini face the cytoplasm. Additionally, NOX2 is stabilized through constitutive interaction with p22phox. The binding of other cytosolic components, such as p40phox and p67phox, to the NOX2/p22phox complex, requires the translocation and interaction of phosphorylated p47phox with NOX2. The GTPase Rac interacts with NOX2 and p67phox during complex building (66), resulting in an active complex that can produce superoxide by transferring an electron from cytosolic NADPH to oxygen on the luminal or extracellular area.

The location of NOX within the cell can range from the plasma membrane to internal compartments, including the secondary and tertiary granules, depending on the type of cell. The first homolog of NOX2 was found to be NOX1, with which it has 60% amino acid similarity. NOX1's subcellular localization depends on cell type and organism. The locations include lysosomal and nuclear membranes and vacuoles, and they may be found in caveolar rafts in vascular smooth muscle cells (64). NOX1 is broadly expressed in a variety of cell types, with the colon epithelium showing the highest levels of expression. The identification of NOX organizer 1 (NOXO1), a homolog of p47phox, and NOX activator 1 (NOXA1), a homolog of p67phox, provided support for the hypothesis that NOX1 function is dependent on cytosolic subunits. NOX1 requires the membrane subunit (p22phox), cytosolic subunits, and the Rac GTPase in order to be activated. NOX3, which share 56% amino acid similarity with NOX2 and was first discovered by Kikuchi *et al*. in 2000 (67), differs in the degree of dependence on the cytosolic subunits. Similar to NOX1 and NOX2, NOX3 is p22phox-dependent, albeit it is unclear whether p22phox has any bearing on NOX3 function *in vivo*. Additionally, several investigations have

established that NOXO1 and NOXA1 are necessary for the activation of NOX3, even though p47phox and p67phox have not been implicated under physiological circumstances, and the significance of Rac in NOX3 activation is still debatable (64,68). NOX4, discovered by Geiszt *et al*. (69) in 2000, and NOX2 have roughly 39% sequence homology. p22phox has a significant impact on NOX4 activity, but cytosolic subunits have little impact (64). Furthermore, Rac's contribution to NOX4 activation is still debatable (70). In vascular smooth muscle cells, NOX4/p22phox interacts with Poldip2, a polymerase (DNA-directed) delta-interacting protein, acting as a positive regulator. Using GST pull-down assays, it has been shown that Poldip2 and p22phox interact and have a synergistic relationship in regulating NOX4 activity. Western blotting, qRT-PCR, and immunohistochemical studies of NOX4-rich organs (such as the aorta, lung, and kidney) show elevated Poldip2 expression. Using siRNA against Poldip2, it has been shown that Poldip2 functions as a positive regulator of NOX4 in conjunction with p22phox in vascular smooth muscle cells (71). NOX5 was discovered by two separate research teams, and it has five different isoforms. Isoforms a, b, c, and d were identified in 1980, while NOX5e or NOX5-S was identified in 1981. The NOX5 isoforms a–d have a lengthy, intracellular N-terminal domain that contains an EF-hand area that binds Ca21, while the fifth isoform lacks the EF-hand region and resembles NOX1-4 structurally (64). The fact that NOX5 isoforms a–d depend on cytosolic calcium for activation rather than p22phox or cytosolic subunits indicates the presence of a Ca21-binding domain. The NOX5e isoform, on the other hand, is dependent on the cAMP response element binding protein for action because it lacks a Ca21-binding domain (72). The dual oxidases (Duox1 and Duox2, also known as thyroid oxidases) have an EF-hand region like NOX5, a NOX homology domain that is comparable to NOX1-4, and a seventh transmembrane that is a peroxidase-like domain at the N-terminus but lacks the few functionally

necessary amino acids. The thyroid gland's dual oxidases were discovered there for the first time in 1999 (64), and they and NOX2 are similar in amino acid composition by about 50%. Duox1 and Duox2 (ThOX1 and ThOX2) have been found to be glycosylated proteins in the plasma membrane and ER, and they both have two N-glycosylation states (73). The maturation factors DuoxA1 and DuoxA2 are necessary for the retention of Duox proteins in the ER (74). Duox2 produces superoxide when it is partially glycosylated and immature, but produces H_2O_2 when it is fully developed (75). There is no direct proof that p22phox is necessary for the activation of Duox proteins, despite prior study showing direct physical contact between these proteins and p22phox (64). Members of the NOX family play a role in the pathogenesis of infections, vascular problems, and poor immunological responses brought on by environmental factors in addition to regulating normal physiological activities.

1.6 Small nucleolar RNAs (snoRNAs)

Lipotoxic stress increases the appearance of small nucleolar RNAs (snoRNAs) in the cytoplasm rather than in the nucleolus, where they are predominantly localized (26). SnoRNAs are non-coding guide molecules that have traditionally played a crucial role in directing the chemical alterations of other RNAs to account for changing cellular requirements (76). SnoRNAs are usually encoded in the introns of the host genes. The majority of snoRNAs in the nucleus are produced by host genes. Following splicing, debranching, and trimming, the mature snoRNAs are subsequently transferred to the nucleolus from the primary transcripts made up of the pre-mRNA of introns (77). Most snoRNAs function by directing how ribosomal RNA (rRNA) and some spliceosomal RNAs are processed and modified post-transcriptionally. Few

snoRNAs have been implicated in the nucleolytic processing of rRNA transcript, in prior studies (78,134).

Small non-coding RNAs called small nucleolar RNAs (snoRNAs) are extensively found in the nucleoli of eukaryotic cells and range in length from 60 to 300 nucleotides. Both protein-coding and non-protein-coding genes' intronic regions are primarily responsible for encoding snoRNAs. Small Cajal RNAs (scaRNAs), H/ACA box snoRNAs, and C/D box snoRNAs are the three main classifications for snoRNAs (79). By adding 2′-O-methylation and pseudouridylation modifications to ribosomal RNA (rRNA) molecules, H/ACA box snoRNAs and C/D box snoRNAs respectively take part in rRNA processing (133). However, a subclass of snoRNAs known as scaRNAs is found near Cajal bodies (CBs). Although scaRNAs follow the C/D-H/ACA classification, certain scaRNAs have both C/D and H/ACA structures (80). Nop1p, Nop56p, Nop58p, and Snu13p are four crucial proteins that C/D box snoRNAs must bind to in order to produce functional small nucleolar ribonucleoproteins (snoRNPs). Similar to this, H/ACA box snoRNAs bind to Cbf5p, Gar1p, Nhp2p, and Nop10p to generate functional snoRNPs.

Eukaryotic C/D box snoRNAs typically have lengths between 70 and 120 nucleotides. The C box and the D box are two conserved sequences found in these snoRNAs. The nucleotides RUGAUGA, which are found at the 5′-end of the snoRNA molecule, make up the C box. The D box, on the other hand, is at the 3′-end and is made up of the nucleotides CUGA (79). These components depend on base pairing between one another to fold into a structure known as a kink-turn. Snu13p detects the kink-turn structure, and Nop1p (known as fibrillarin (FBL)), Nop58p, and Nop56p are then recruited for 2′-O methylation modification (81, 82).

The pseudouridylation pockets, which are seen in H/ACA snoRNAs and are typically 60–75 nucleotides in length, are where uridine residues on the substrate RNA are isomerized. Cbf5p serves as the catalytic protein involved in pseudouridylation, and H/ACA box snoRNPs bind to it as well as Nop10p, Gar1p, and Nhp2p (83). The H box and the ACA box, which are situated downstream of the first and second hairpins, respectively, are two conserved sequences found in eukaryotic H/ACA box snoRNAs (83). Additionally, certain snoRNAs have been identified as orphan snoRNAs since they appear to have no complementarity with rRNAs at known modified sites. These demonstrated that snoRNAs are capable of more than only 2′-O methylation and rRNA pseudouridylation. As research on snoRNA progresses, new snoRNA functions continue to expand. These emerging functions include producing bioactive RNA species (135), functioning as molecular scaffolds for RNA-protein complexes, regulating protein activities by modulating subunit interactions and guiding proteins to recognize and bind target molecules (136). Other emerging functions include participating in DNA damage response (135) and regulating gene expression, including their host gene expression.

1.7 Rationale

SnoRNAs and NOX had been implicated as critical mediators in the propagation of oxidative stress and cell death in response to lipotoxicity in prior studies. Recently, it was shown that cultured cells with knocked-down box H/ACA *SNORA73* snoRNAs encoded within the small nucleolar RNA hosting gene-3 manifested resistance to lipid-induced cell death and oxidative stress (45). Another prior study by Holley *et al*. (84) showed that doxorubicin-induced oxidative stress significantly increased cytosolic snoRNA levels within H9c2 rat cardiomyocytes. A reduction in snoRNA accumulation was observed in NOX4 siRNA-mediated

knockdown cells. The research group of Wang *et al*. (85) reported that NOX inhibitors (NOXi) attenuated LPL lipoprotein hydrolysis products (HPs)-induced ROS production.

In addition to prior studies, our laboratory reported an upregulation of 63 snoRNA transcripts and a reduction in the amount of 18S and 28S ribosomal RNAs in macrophages incubated with lipid HPs generated by LPL (86). All data taken together suggest a link between lipid HPs-induced ROS production, overexpression of snoRNAs, and NOX activity. Thus, my research aims to address this link.

1.8 Research objective

My primary research objective was to determine if there will be a change in LPL hydrolysis products-induced ROS production with or without NOXi in macrophages.

My secondary objective was to determine if NOX-induced ROS is an effector of lipid hydrolysis product-mediated snoRNA overexpression.

1.9 Hypothesis

I hypothesized that Lp hydrolysis products produced by LPL lead to NOX-mediated oxidative stress within macrophages that can be inhibited using NOXi. I further hypothesized that snoRNA expression would increase due to NOX activity in macrophages incubated with Lp hydrolysis products produced by LPL.

1.10 Significance

Atherosclerosis is promoted by LPL expression in macrophages. Previous research from has demonstrated that Lp HPs produced by LPL change gene transcription and cell signaling pathways, which may affect the cellular activities of macrophages. This investigation will establish whether NOX is a mediator in generating ROS, malondialdehyde (MDA) and the increase in snoRNAs expression by Lp HPs in macrophages. Understanding NOX functions and how LPL HPs affect NOX activity will provide insights into atherosclerosis development and new drug targets for the treatment of atherosclerosis.

CHAPTER 2: MATERIALS AND METHODS

2.1 HEK-293 Transfection with Recombinant LPL Plasmid

2.1.1 Human LPL plasmid generation

The plasmid pcDNA3.LPL (a pcDNA3 vector that contains the human LPL cDNA [GenBank: NM_000237]) was a gift from Dr. Daniel Rader (Perelman School of Medicine, University of Pennsylvania, PA, USA). For transformation, 50 ng of pcDNA3.LPL was added to 200 µL of competent DH5α *Escherichia coli* cells (cat. #60107-1-LU, Lucigen, Middleton, WI, USA) and mixed. The mixture was mixed then kept on ice for 20 minutes. The mixture was then incubated at 42˚C for 90 seconds. After the incubation at 42˚C, the DH5α competent cells mixture was placed on ice for 1 minute. A total volume of 800 µL of lysogeny broth (LB) (cat. #L3522, Sigma-Aldrich, St. Louis, MO, USA) was added to the DH5α competent cells mixture and incubated at 37˚C in a Barnstead MaxQ 4000 Orbital Incubator Shaker (Thermo Fisher Scientific, Waltham, MA, USA) at 200 rpm for 40 minutes. Fifty µL of transformed DH5α cells were spread on LB agar (cat. # BP1425-500, Fisher BioReagents, Fisher Scientific, Waltham, MA, USA) containing 50 µg/mL ampicillin (cat. # A9518, Sigma-Aldrich, St. Louis, MO, USA) in 100 mm cell culture dishes (cat. # 353003, Falcon®, BD Biosciences, Franklin Lakes, NJ, USA) and were incubated at 37˚C for 18 hours. Once the incubation was over, a colony from the LB agar culture plate was taken and inoculated in 3 mL of LB broth with 3 µL of 50 mg/mL ampicillin in a Samco™ Disposable Culture Tube 17 × 100 mm (cat. # 17-010, Thermo Fisher Scientific, Waltham, MA, USA). The cells were then incubated at 37˚C in a Barnstead MaxQ

4000 Orbital Incubator Shaker at 200 rpm for 16 hours. Once the incubation was completed, the DH5α cell culture was centrifuged at 3400 ×*g* in 50 mL tubes in a Multifuge X1 R Package (cat. # 97039-578, Thermo Fisher Scientific, Waltham, MA, USA) for 10 minutes at room temperature. The supernatant was removed and discarded. The pcDNA3.LPL plasmid extraction and purification from the bacterial pellet were carried out using the ZymoPURE^{TM} Plasmid Miniprep Kit (cat. # D4209, Zymo Research Corporation, Irvine, CA, USA) according to the manufacturer's instructions. The resulting pcDNA3.LPL plasmid was stored at -20˚C until required.

2.1.2. HEK-293 cell culture and maintenance

Human embryonic kidney (HEK) 293 cells from the American Type Culture Collection (ATCC) (cat. # CRL-1573, Manassas, VA, USA) were thawed and cultured with Dulbecco's Modified Eagle Medium (DMEM) growth media made up of 4.5 g/L glucose, 3.7 g/L sodium bicarbonate, 584 mg/L L-glutamine, and 110 mg/L sodium pyruvate (cat. #SH30022.01, Cytiva, Marlborough, MA, USA) in T75 culture flasks (cat. #C353136, Corning Life Sciences, Corning, NY, USA). Prior to the HEK-293 cells culturing, the DMEM media had been supplemented with 1% *v/v* antibiotic/antimycotic (A/A) (cat. #15240062, Gibco™, Thermo Fisher Scientific, Waltham, MA, USA) and 10% *v/v* fetal bovine serum (FBS) (cat. #16000044, Gibco™, Thermo Fisher Scientific, Waltham, MA, USA). The incubation of the HEK-293 cells was carried out at 37°C with 5% CO_2 (gas). The spent medium was removed once the cell's confluency reached about 80-90% confluency. The adhered HEK-293 cells in the flask were then carefully washed with 4 mL of DMEM media (FBS-free). The cells were treated with 1 mL of 0.25% (*w/v*)

trypsin-ethylenediaminetetraacetic acid (EDTA) (#25200056, Gibco™, Thermo Fisher Scientific, Waltham, MA, USA) after washing and were incubated for 5 minutes at 37°C to allow the cells to detach from the surface of the flask. After the incubation with trypsin, 4 mL of DMEM (+FBS, +A/A) was added to the culture flask and pipetted vigorously to break the clumps and suspend the cells. One mL of the suspended cells was pipetted into a new T75 flask with 14 mL of conditioned DMEM growth media and incubated at 37˚C with 5% CO_2 (gas) for a new passage cycle, while 4×10^6 cells in 10 mL supplemented media were seeded into 100-mm culture dishes in preparation for transfection.

2.1.3. HEK-293 cell transfection

Suspended HEK-293 cells in supplemented DMEM (+FBS, +A/A) were counted (as seen in section 2.3.2), and 4 x10^6 cells were seeded into 100-mm culture dishes (as seen in section 2.1.2). Between 70% and 90% confluency was seen after 24 hours of incubation of the cells at 37°C with 5% CO_2 (gas). Following 24 hours of incubation, spent media was replaced with 12 mL of supplemented DMEM and 3 mL of dilution media made up of 1.5 mL of Opti-MEM™ Reduced Serum Medium (cat. # 31985070, Gibco™, Thermo Fisher Scientific, Waltham, MA, USA) containing 20 µL of Lipofectamine™ 2000 Transfection Reagent (cat. # 11668027, Invitrogen™, Thermo Fisher Scientific, Waltham, MA, USA) and 1.5 mL of Opti-MEM reduced serum media with either 10 ug of pcDNA3.LPL plasmid or 10 ug of pcDNA3, empty vector, generated in section 2.1.1. The media were gently mixed by rocking the cell culture plate back and forth. The cells were then incubated at 37°C with 5% CO_2 (gas) for 24 hours. The cells were washed with FBS-free DMEM following the 24 hours of incubation and were incubated with 4

mL of heparinized DMEM containing 1% *v/v* A/A and 10 U/mL of heparin (cat. # H3149, Sigma-Aldrich, St. Louis, MO, USA) for 23.5 hours at 37°C with 5% CO_2 (gas). The heparin results in the release of LPL into the medium by displacing LPL produced by the cells into the medium. After 23.5 hours of incubation, cells were further treated and incubated with an additional 1 mL of heparinized DMEM containing 1% *v/v* A/A and 100 U/mL of heparin for 30 minutes at 37°C with 5% CO_2 (gas). At the end of 30 minutes, the media were collected and spun at 125 ×*g* for 5 minutes at 4°C to remove cell debris and divided into aliquots. Aliquots were stored immediately at -80°C.

2.2. Qualitative and quantitative analysis of LPL

2.2.1. SDS-PAGE and western blot analysis

Sodium dodecyl sulfide polyacrylamide gel electrophoresis (SDS-PAGE) was carried out to investigate the expression of LPL by the pcDNA3.LPL transfected cells and control cells (empty vector pcDNA3). The heparinized media collected in section 2.1.3 were analyzed. Thirty percent acrylamide:bis-acrylamide solution (cat. #1610156, Bio-Rad Laboratories, Hercules, CA, USA) was used to prepare a 12% *w/v* resolving gel and a 4% *w/v* stacking gel according to the manufacturer's instructions. Blue juice lysis buffer at 4x concentration (50% *v/v* glycerol, 6% *v/v* β-mercaptoethanol, 10% *w/v* SDS, and 0.01% *w/v* bromophenol blue) was warmed, and 12 µL was added to 36 µL of the heparinized media sample. The samples were heated at 95°C for 5 minutes, and 20 µL of each sample was loaded onto the SDS-PAGE gel.

The SDS-PAGE gel was run using a Tris-glycine-SDS running buffer (25 mM Tris, 192 mM glycine, and 0.1% SDS) with a pH of 8.3 (cat. #1610772, Bio-Rad Laboratories, Hercules, CA, USA) at 120 volts for 1 hour. Following the SDS-PAGE, proteins were transferred onto nitrocellulose membrane (cat. #1620115, Bio-Rad Laboratories, Hercules, CA, USA) with cold transfer buffer made up of 25 mM Tris, 192 mM glycine, and 20 % *v/v* methanol (cat. #A412-4, Thermo Fisher Scientific, Waltham, MA, USA) at 100 volts, 350 mA for 1 hour. The membrane, after transfer, was incubated in a blocking solution made up of 5% *w/v* bovine serum albumin (BSA) (cat. #A7906, Sigma-Aldrich, St. Louis, MO, USA) in 1X Tris-buffered saline with 0.05% *v/v* Tween-20 (cat. # P9416, Sigma-Aldrich, St. Louis, MO, USA) (TBST) at room temperature for 1 hour on a rocking platform, Model 100 (VWR International, Radnor, PA, USA). Following the blot blocking, primary antibody incubation was carried out by incubating the membrane in a 1:1,000 dilution of a polyclonal anti-human LPL antibody (cat. # sc-32885, Santa Cruz Biotechnology, Dallas, TX, USA) in 5% BSA with 0.05% *w/v* sodium azide (cat. # 190380050, Thermo Scientific Chemicals, Waltham, MA, USA) in TBST, overnight at 4°C on a rocking platform. After the primary incubation, the membrane was washed for 10 minutes with 20 mL of TBST on a rocking platform. Secondary antibody incubation commenced after five washings of the membrane. The membrane was incubated with 1:2,000 dilution of horseradish peroxidase-conjugated anti-rabbit IgG (cat. # SA1-200, Pierce Biotechnology, Rockford, IL, USA) in 5% BSA in TBST and incubated for 1 hour on a rocking platform. Following secondary antibody incubation, the membrane was washed four times for 10 minutes each with TBST on a rocking platform. Finally, the membrane was incubated with the ECL™ Western Blotting Detection Kit reagent (cat. # RPN2232, Cytiva, Chicago, IL, USA) for protein visualization, according to the manufacturer's instructions. The ChemiDoc MP Imaging System (Bio-Rad

Laboratories, Hercules, CA, USA) was used to detect both the colorimetric and chemiluminescence images of the blot.

2.2.2. LPL activity assay

LPL activity was analyzed using 1, 2-*O*-dilauryl-*rac*-glycero-3-glutaric-resorufin ester (cat. # D7816, Sigma-Aldrich, St. Louis, MO, USA) as substrate, as previously described (87). In brief, substrate stock solution (2 mg/ml) was prepared by dissolving 2 mg of 1,2-O-dilauryl-rac-glycero-3-glutaric acid-resorufin ester in 1 ml of 1,4-dioxane (cat. # 296309, Sigma-Aldrich, St. Louis, MO, USA); the substrate stock was stored at 4˚C until required. In triplicate, 75 µL of heparinized media with or without LPL collected from the transfected HEK-293 cells (as seen in section 2.1.3) was added to 105 µL of a lipase assay buffer (20 mM Tris, 1 mM EDTA, pH 8.0) in a clear, lidless and non-sterile 96 well plate (cat. # 2205, Thermo Fisher Scientific, Waltham, MA, USA). Twenty µLs of 0.3 mg/mL resorufin ester substrate, from the dilution of the substrate stock solution (2 mg/ml) with lipase assay buffer, was added to each sample well containing LPL or control media. The absorbance of the plate was read at 572 nm every 3 minutes for 1 hour at 37˚C using the Synergy Mx Multi-Mode Microplate Reader (BioTek Instruments, Winooski, VT, USA). The standard curve was obtained by diluting 400 µM resorufin ester standard stock in lipase assay buffer to make 200 µL of 0, 1, 2, 3, 4, 6, 10, 15, 20, and 40 µM concentrations. The slope from the standard curve was used to calculate the concentration of resorufin released by the LPL and control samples. The concentration of resorufin formed was plotted over time (60 minutes). The lipase activity was calculated using the initial velocity from the kinetic graph (figure S2) during the linear phase of the reaction.

2.3. Lipoprotein hydrolysis products generation, quantification, and incubation with THP-1 macrophages.

2.3.1. THP-1 monocyte cell culture and differentiation

THP-1 monocytic cells (cat. # TIB-202, American Type Culture Collection, Manassas, VA, USA) were grown in T75 culture flasks (cat. #C353136, Corning Life Sciences, Corning, NY, USA) with Roswell Park Memorial Institute (RPMI)-1640 media containing 25 mM HEPES and 0.3 mg/L L-glutamine (cat. # SH30255.01, Cytiva, Marlborough, MA, USA) and supplemented with 1% *v/v* A/A (#15240062, Gibco™, Thermo Fisher Scientific, Waltham, MA, USA) and 10% *v/v* FBS (#16000044, Gibco™, Thermo Fisher Scientific, Waltham, MA, USA). The cells were incubated for 96 hours at 37°C with 5% CO_2 (gas). Three mL of the cell suspension was passaged into a new T75 flask with 12 mL of supplemented RPMI-1640 growth media and incubated at 37˚C with 5% CO_2 (gas). After growing the THP-1 cells to a concentration of 8×10^5 to 1×10^6 cells/mL, the cell suspension was spun down at 1000 ×*g* for 5 minutes in preparation for the cell differentiation. After centrifugation, 5 mL of supplemented media (RPMI-1640) was added to the cell pellets and properly mixed after the supernatant had been carefully discarded. After counting the number of cells using a hemocytometer (see section 2.3.2), 100 µL of 1×10^4 cells/mL were seeded into a clear-bottom, dark 96-well polystyrene microplate (cat. # 3603, Corning Incorporated, Corning, NY, USA) for the ROS test along with 100 nM phorbol 12-myristate-13-acetate (PMA) (cat. # 79346, Sigma-Aldrich, St. Louis, MO, USA). For the thiobarbituric acid reactive substance (TBARS) assay and RNA isolation, 100

nM PMA was added to 1 mL of 1×10^6 cells/mL in 6-well Clear TC-treated Multiple Well Plates (cat. # 3516, Corning Incorporated, Corning, NY, USA).

The cells were washed with RPMI 1640 Medium without phenol red (cat. # 11835030, Thermo Fisher Scientific, Waltham, MA, USA) without FBS and A/A three times after 48 hours of incubation with PMA. After washing, the cells were incubated with RPMI 1640 media containing 0.2% *w/v* fatty acid free-bovine serum albumin (FAF-BSA) (cat. # A4612, Sigma-Aldrich, St. Louis, MO, USA), 1% *v/v* A/A, and 100 nM PMA for 24 hours. The cells were then incubated for 1 hour with RPMI-1640 media supplemented with 0.2 % *w/v* FAF-BSA, 1% *v/v* A/A, 100 nM PMA, and 25 μg/mL tetrahydrolipstatin (THL) (cat. # O4139, Sigma-Aldrich, St. Louis, MO, USA) dissolved in dimethyl sulfoxide (DMSO) (cat. # D8418,, Sigma- Aldrich, St. Louis, MO, USA). The purpose of adding THL to the cells is to inhibit endogenous lipase activity.

2.3.2. Cell counting using trypan blue exclusion assay

Trypan Blue was used to count the live cells prior to LPL HPs or non-HPs treatment. After four days of passaging, the monocyte cells were transferred into a 15 mL centrifuge tube and centrifuged for five minutes at 1000 ×*g*. The supernatant was discarded. After the supernatant was removed, 5 mL of RPMI medium supplemented with 10% FBS and 1% A/A was added to the cell pellets and thoroughly mixed together. 10 μL of cell suspension and 10 μL of 0.4% (*w/v*) trypan blue (cat # 25-900-CI, Corning Incorporated, Corning, NY, USA) were combined in a different microfuge tube. After that, the cells were put into a hemocytometer, and live cells were counted under a microscope in a designated region.

The cell seeding density in cells per mL was calculated using the formula below:

$$\text{Seeding Density} = (\#\text{ of cells in four quadrants} \times 2 \times 10^4)/4 \qquad \text{(equation 1)}$$

2.3.3. Lipoproteins

VLDL isolated from human plasma (cat. # 365-10, Medix Biochemica, Espoo, Finland), with a triglyceride content of 14,120 mg/dL and total cholesterol of 5,300 mg/dL, was purchased and stored at -80°C until required.

2.3.4. Lipoprotein hydrolysis by LPL

The VLDL with a 2.7 triglyceride/total cholesterol ratio (see section 2.3.3) was mixed with heparinized media containing LPL or control in a 1:1 ratio to generate lipoprotein hydrolysis products. The mixture was incubated at 37°C for 4 hours and put on ice right after incubation. The quantification of FFA released from the lipoprotein was determined at different time slots, including 0 hours, 0.5 hours, and 4 hours (see section 2.3.5). Lastly, THP-1 macrophages were treated with the lipoprotein hydrolysis product generated by LPL or control diluted with media to an FFA concentration of 0.25 mM (see section 2.3.6).

2.3.5. FFA quantification from lipoprotein HPs

Following the manufacturer's instructions, the NEFA-HR (2) enzymatic colorimetric assay kit (cat. # 999-34691 (Color Reagent A), 995-34791 (Solvent A), 991-34891 (Color Reagent B), 993-35191 (Solvent B), FUJIFILM Wako Chemicals U.S.A. Corporation,

Richmond, VA, USA) was used to measure the total FFA concentration produced from lipoprotein hydrolysis by LPL. Briefly, 4 µL of diluted LPL hydrolysis products or control hydrolysis products (hydrolysis products were diluted with RPMI-1640 in ratio 1:10) were pipetted into a well in a transparent, lidless, non-sterile 96-well plate (cat. #14-245-71, ThermoFisher Scientific, Waltham, MA, USA). A NEFA standard solution (1 mM oleic acid) was included in the kit as a reference standard. This solution was diluted to a final volume of 4 µL in separate wells using distilled H_2O at 0, 0.5, 0.75, 1, 1.5, 2, or 4 µL of the NEFA standard solution. Two hundred and twenty-five µL of Solvent A from the kit was added to all samples and standard wells, and the plate was incubated at 37˚C for 10 minutes. After incubation, 75 µL of Solvent B was added to all the wells, and they were incubated for 10 minutes at 37˚C. The absorbance of the samples and standards were measured at 550 nm at 37˚C using a Synergy Mx Multi-Mode Microplate Reader (BioTek Instruments, Winooski, VT, USA). The concentration of FFA in each sample, including LPL hydrolysis products or control hydrolysis products, was determined using the standard curve.

2.3.6. THP-1 macrophage treatment with lipoprotein HPs

Lipoprotein hydrolysis products generated by LPL, see section 2.3.4, were diluted to 0.25 mM (non-esterified fatty acid concentration) with RPMI-1640 supplemented with 0.2% w/v FAF-BSA, 1% *v/v* A/A, 25 µg/mL tetrahydrolipstatin, and 100 nM PMA. Lipoprotein lipid hydrolysis products that may have been present in the heparinized media from cells transfected with pcDNA (control) were diluted to mimic the diluted volumes of the 0.25 mM lipoprotein hydrolysis products by LPL. After THP-1 cells were differentiated, incubated with THL, and

washed with plain RPMI-1640 (see section 2.3.1), lipoprotein hydrolysis products generated by LPL with or without NOXi (100 μM of apocynin or 20 μM of GKT136901 diluted in DMSO) prepared above were added to the cells and incubated for 18 hours at 37°C with 5% CO_2 (gas) for RNA isolation and TBARS assay. The cells deemed for ROS assay were incubated with lipoprotein hydrolysis products by LPL diluted to 0.25 mM with RPMI-1640 media without phenol red supplemented with 0.2% w/v FAF-BSA, 1% *v/v* A/A, 25 μg/mL tetrahydrolipstatin, and 100 nM PMA for 4 hours at 37°C with 5% CO_2 (gas) after DCFDA staining (see section 2.4.1).

2.4. Analysis of THP-1 macrophage cell oxidative stress

2.4.1. Measurement of ROS using the DCFDA (2',7'-dichlorofluorescin diacetate) - Cellular ROS Assay.

ROS generated by THP-1 macrophages in the presence or absence of Lp hydrolysis products by generated LPL with or without NOXi and control over 4 hours (see section 2.3.6) was measured using the DCFDA / H2DCFDA - Cellular ROS Assay Kit (cat. # ab113851, Abcam, Cambridge, UK). Thirty minutes prior to the commencement of the 4-hour hydrolysis products treatment, 100 μL of 20 μM of DCFDA diluted with RPMI-1640 (cat. # 11835030, Thermo Fisher Scientific, Waltham, MA, USA) was added to the differentiated cell that had been incubated with fatty acid-free medium (RPMI-1640 supplemented with 0.2% w/v FAF-BSA, 1% v/v A/A, 25 μg/mL tetrahydrolipstatin, and 100 nM PMA) for 24 hours, and washed with plain RPMI-1640. Following the 30 minutes of DCFDA staining and the removal of excess dye with

plain RPMI-1640, the cells were then treated with the lipoprotein hydrolysis products for 4 hours. 100 µL of supplemented RPMI-1640 media containing 100 µM *tert*-butyl hydroperoxide (TBHP) was added to three wells and incubated at 37°C for 4 hours as positive controls. TBHP was provided with the cellular ROS assay kit. Blank wells were prepared with treatment media without cells. The fluorescence intensity of the cells was measured immediately after 4 hours using Synergy Mx Multi-Mode Microplate Reader (BioTek Instruments, Winooski, VT, USA) at Ex/Em = 485/535 nm in endpoint mode and corrected by subtracting the blank wells' fluorescence from each sample's fluorescence. The corrected fluorescence intensity of the cells is proportional to the ROS generated. The DCFDA in the ROS detection kits is a fluorescent probe that quantifies ROS in live cells. Upon entering the cells, the DCFDA acetate group gets cleaved by cellular esterases yielding non-fluorescent DCFH. ROS converts the DCFH to fluorescent DCF upon oxidation.

2.4.2. Measurement of Malondialdehyde (MDA) with TBAR assay

The MDA generated by THP-1 macrophage cells and media was measured after an 18-hour treatment with lipoprotein hydrolysis products in a 6-well plate using a TBARS Parameter Assay Kit (cat. # KGE013, R&D Systems, Inc., Minneapolis, MN, USA). Cell culture media were collected after 18 hours of treatment and stored at -80°C until further use. Once the media was collected, the cells were washed twice with cold PBS and lysed using 5-fold diluted cell lysis buffer 3 (R&D Systems Inc.). One mL of diluted cell lysis buffer 3 was added to 1×10^6 cells, and the cells were incubated at 4 °C for 30 minutes with gentle agitation. Following 30 minutes of incubation, the cell lysates and the cell media were prepared for TBARS assay by

adding 300 µL of each sample to 300 µL TBARS acid reagent in microcentrifuge tubes and incubated for 15 minutes at room temperature. The microcentrifuge tubes were centrifuged at ≥ 12,000 ×*g* for 4 minutes after incubation, and the supernatant was collected for the TBARS assay.

MDA standard stock solution was prepared by adding 100 µL of TBARS Standard to 200 µL of TBARS acid reagent (supplied in the kit). The MDA standard stock solution was allowed to sit for 30 minutes at room temperature with gentle agitation, which resulted in a 167 µM MDA stock solution. The MDA standard stock solution was diluted after the 30-minute agitation to 16.7, 8.35, 4.18, 2.09, 1.04, 0.52, 0.26, and 0 µM with deionized water. A standard curve was plotted and used to determine the concentration of MDA formed in the cells and media samples.

Lastly, 150 µL of standards and samples were added to each well of the microplate provided with the kit. Seventy-five µL of thiobarbituric acid (TBA) reagent was added to all standard and sample wells. The optical density of each well was pre-read using Synergy Mx Multi-Mode Microplate Reader at 532 nm and at a temperature of 37°C. The adhesive strip provided was used to cover the microplate, which was incubated for 3 hours at 47 °C. The final optical density of each well was read at 532 nm at 47°C. The amount of MDA generated was determined by subtracting the optical density pre-reading from the final reading.

2.5 RNA preparation, cDNA synthesis, and gene expression

2.5.1 RNA isolation, genomic DNA removal and RNA clean-up

RNA was isolated from macrophages treated with lipoprotein hydrolysis products by LPL, with or without NOXi, or control (pcDNA) for 18 hours (see section 2.3.6). Following the 18 hours of incubation, the spent media was discarded, and 1 mL of TRIzol® Reagent (cat. # 15596018, Invitrogen, ThermoFisher Scientific, Waltham, MA, USA) was pipetted into each well. Following a thorough lysing of the cells in TRIzol®, the cells were transferred into 1.5 mL Eppendorf tubes. Two hundred µL of chloroform was added to the samples containing 1 mL of TRIzol® and mixed thoroughly. The mixture was centrifuged for 15 minutes at 4˚C at 12,000 × *g* using a Legend Micro 21 R centrifuge (ThermoFisher Scientific, Waltham, MA, USA). Three phases were obtained by centrifugation: a protein-containing lower organic phase, a DNA-containing interphase, and an upper aqueous phase containing RNA.

The RNA-containing upper aqueous phase was transferred to a new tube, and 500 µL of isopropanol was added to it. The mixture was incubated for 10 minutes at 4˚C. Using a Legend Micro 21 R centrifuge (ThermoFisher Scientific, Waltham, MA, USA), the mixture was centrifuged at 12,000 × *g* at 4˚C for 10 minutes. After the supernatant was removed, contaminants were removed by adding 1 mL of 75% ethanol to the RNA pellets and centrifuging the sample at 7,500 × *g* for 5 minutes at 4˚C. The supernatant was removed, and the ethanol was air-dried. Forty µL of nuclease-free water was added to resuspend the RNA pellet aided by gentle tapping on the tube. The RNA concentration and purity were measured using a NanoDrop

2000 spectrophotometer (ThermoFisher Scientific, Waltham, MA, USA). Following RNA isolation, genomic DNA contamination was removed by treating the isolated RNA with the TURBO DNA-free™ Kit (cat. # AM1907, Invitrogen, Thermo Fisher Scientific, Waltham, MA, USA) following the manufacturer's instructions. The RNA concentration was, again, measured after DNase treatment. The RNA quality before and after DNase treatment was checked using a 1% agarose gel and RNA samples were stored at -80˚C until further use. The RNA integrity of the total RNA samples was assessed using an Agilent 2100 Bioanalyzer at The Centre for Applied Genomics (Toronto, Canada).

2.5.2 cDNA synthesis

To synthesize 500 ng of cDNA in 10 µL reaction volume from 500 ng of RNA, 500 ng of RNA samples from section 2.5.1 were made up to 5 µL with nuclease-free H_2O in PCR tubes and placed on ice. Master mix A and master mix B were freshly prepared for each set of samples in 1.5 mL microcentrifuge tubes. Master mix A contained 1 µL of random primers (3 µg/µL) (cat. # 48190011, Invitrogen, ThermoFisher Scientific, Waltham, MA, USA) and 0.5 µL of deoxyribonucleotide triphosphate mix (10 mM) (cat. # R0192, Thermo Fisher Scientific, Waltham, MA, USA). Master mix B contained 2 µL of 5X First-Strand Buffer (Invitrogen, ThermoFisher Scientific, Waltham, MA, USA), 1 µL of 0.1 M dithiothreitol, and 0.5 µL of RNaseOUT™ Recombinant Ribonuclease Inhibitor (40 U/µL, cat. # 10777019, Invitrogen, ThermoFisher Scientific, Waltham, MA, USA). To each tube containing 5 µL of 500 ng RNA samples, 1.5 µL of master mix A was added, mixed thoroughly, and incubated at 65˚C for 5 minutes in an Eppendorf PCR machine (Eppendorf AG, Hamburg, Germany). Following the 5

minute incubation, the samples were quickly chilled on ice and spun down. 3.5 µL of master mix B was then pipetted into each tube, mixed thoroughly, and the samples were further incubated at 37˚C for 2 minutes. Finally, 0.5 µL of M-MLV reverse transcriptase (200 U/µL) (catalog number 28025013, Invitrogen, Thermo Fisher Scientific, Waltham, MA, USA) was added and mixed gently to the samples in each tube. The RNA sample mixtures were then incubated at the following temperatures: 25˚C for 10 minutes, 37˚C for 50 minutes, 72˚C for 10 minutes. The reaction was stopped at 4˚C. The resulting cDNA samples with a concentration of 50 ng/µL were stored at -20°C until further use.

2.5.3 Quantitative PCR (qPCR) analysis

The relative gene expression of *SNORA80E*, *SNORA60*, and *SNORA56* was measured in THP-1 macrophages treated with lipoprotein hydrolysis products by LPL, using SsoAdvanced Universal SYBR Green Supermix (Bio-Rad), according to manufacturer's instructions. Normalization of expression was to the expression of *ACTB*. Forward and reverse primers (Table 3) were synthesized by Integrated DNA Technologies (Coralville, IA, USA). The amplification efficiencies of the aforementioned genes were carried out as described by Pfaffl *et al.* (88).

Table 3: Primers used for real-time PCR with their amplification efficiencies.

Gene (Accession Number)	**Primers (Start/end Nucleotide)**	**Amplification efficiency**
ACTB NC_000007.13	Forward: (349) 5'-ACC TTC TAC AAT GAG CTG CG-3' (368)	2.14

	Reverse: (537) 5'-CCT GGA TAG CAA CGT ACA TGG-3' (517)	
SNORA80E NR_002974.1	Forward: (24) 5'-CTT CTC TGT GGG CCT CTC AT-3' (43) Reverse: (97)5'-TAA GGG GAC TGG GCA ATG GT-3' (78)	1.92
SNORA60 NR_002986.1	Forward: (31) 5'-CTG TGC TCT GGT CAT CAA TAA-3' (52) Reverse: (131) 5'-GAA AGC GCC AGC ATT TGA-3' (113)	2.17
SNORA56 NM_001288747.1	Forward: (1794) 5'-TTC TAG TCT GGC TCG TGG GA-3' (1813) Reverse: (1897) 5'-TGG CAA GTC TAA AGC CAC CA-3' (1878)	0.97*

* Information obtained from (Thyagarajan, 2017) (86)

To determine amplification efficiencies, briefly, cDNA synthesized from THP-1 macrophages treated with lipoprotein hydrolysis product by LPL (with or without GKT136901) and control were pooled together. Ten µL of SsoAdvanced Universal SYBR Green Supermix (cat. # 1725270, Bio-Rad Laboratories, Inc., Hercules, CA, USA) and 1 µL of each gene primer (forward and reverse primers) (10 µM) were added to 50 ng, 10 ng, 2 ng, 0.4 ng, 0.08 ng, and 0.016 ng of the pooled cDNA. The mixture was made up to 20 µL with an appropriate volume of nuclease-free H_2O (cat. # FERR0581, Thermo Fisher Scientific, Waltham, MA, USA). qPCR was carried out using a CFX96^{TM} Real-Time PCR detection system (Bio-Rad Laboratories, Inc., Hercules, CA, USA) following this Real-time PCR cycle conditions: 1 cycle of 95°C for 3 minutes, and 40 cycles of 95°C for 15 seconds, 59.5°C for 15 seconds, and 72°C for 20 seconds. Threshold cycle (Ct) values for each aforementioned gene were plotted against Log cDNA

concentrations used. Amplification efficiency was calculated using the slope from the graph in the following equation:

$$E = 10[-1/\text{slope}] \qquad \text{equation 2}$$

E denotes amplification efficiency in the equation.

The qPCR reactions were performed in triplicate to measure efficiency. Each gene amplification reaction's melting curve showed that only one product was amplified. Following amplification efficiency reactions, the gene expression analysis for target genes was carried out by calculating the fold change in relative expression as previously described (8). Briefly, to assess the expression of *SNORA56*, *SNORA60*, and *SNORA80E* in VLDL HPs by LPL-treated macrophages; 2 ng, 20 ng, and 25 ng of cDNA from control and treated macrophages, respectively, 10 µL of SsoAdvanced Universal SYBR Green Supermix (Bio-Rad) and 1 µL of each gene primer (forward and reverse primers) (10 µM) were added and made up to 20 µL total reaction volume with nuclease-free H_2O. Reactions were performed in triplicate, and target genes were normalized to *ACTB*.

The relative expression ratio of each target gene was measured using the Pfaffl *et al.* mathematical model:

$$\text{Fold change} = \frac{(E_{target})^{\Delta Ct_{target}\ (CONTROL - TEST)}}{(E_{reference})^{\Delta Ct_{reference}\ (CONTROL - TEST)}} \quad \text{equation 3}$$

where Etarget and Ereference represent the amplification efficiency of the target genes and *ACTB*, respectively. ΔCt_{target} (CONTROL - TEST) refers to the difference in Ct values of target genes between the control and treated macrophages, while $\Delta Ct_{reference}$ (CONTROL - TEST) refers to the difference in Ct values of reference gene between the control and treated macrophages, respectively.

2.6 Statistical analysis

Standard deviation (SD) was determined, and an unpaired student's t-test or Tukey test was performed to determine the statistical significance of the data.

CHAPTER 3: RESULTS

3.1 Enzymatic activity and immunoblot of recombinant human LPL expressed in the heparinized media of pcDNA3-hLPL-transfected HEK-293 cells

Active recombinant human LPL was present in the heparinized media of pcDNA3-hLPL-transfected HEK-293 cells. Western blot analysis was carried out to investigate the expression of LPL by the pcDNA3-hLPL-transfected cells and control-transfected cells (with empty vector pcDNA3). The expression of LPL was observed in the heparinized media of pcDNA3-hLPL-transfected cells as an approximately 58 kDa band in the western blot analysis gel image (Figure 7A). In contrast, the heparinized media of the control-transfected cells showed no band. An approximately 31 kDa band, a likely cleaved fragment of LPL, can be seen on the LPL lane. In a full-length LPL, the linker region between its N-terminal catalytic domain and C-terminal lipid binding domain can be cleaved by proprotein convertases (140). A similar 31 kDa band was previously observed in our laboratory (Noel, Pickett, & Brown, unpublished, 2017).

The heparinized media collected from the pcDNA3-hLPL-transfected and control-transfected cells were assessed for enzymatic activity using the 1,2-O-dilauryl-*rac*-glycero-3-glutaric-resorufin ester as substrate. Lipase activity is proportional to the initial rate of methyl resorufin formation at the beginning of the reaction when it increases linearly with time. The pcDNA3-hLPL-transfected cells' heparinized media showed significantly higher enzymatic activity, 7166.22 µmol/mL/min, than the control-transfected cells' heparinized media, 2746.67µmol/mL/min (Figure 7B).

Once the expressed LPL had been confirmed to be active, VLDL, with a triglyceride content of 14,120 mg/dL and total cholesterol of 5,300 mg/dL, was incubated with heparinized media from either pcDNA3-hLPL-transfected cells or control cells for 4 hours at 37°C. The FFA

amount released by LPL from VLDL after 4 hours of incubation (12.065 ± 0.948 nmol/μL) was significantly higher than the FFA amount released from VLDL treated with the control-transfected cells heparinized media (7.393 ± 0.715 nmol/μL) (Figure 8).

Figure 7

A.

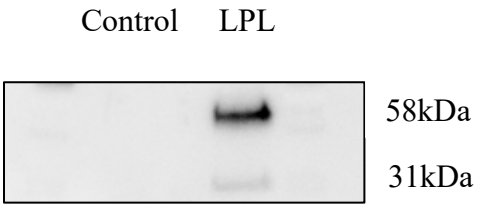
Control
LPL
58kDa
31kDa

B.

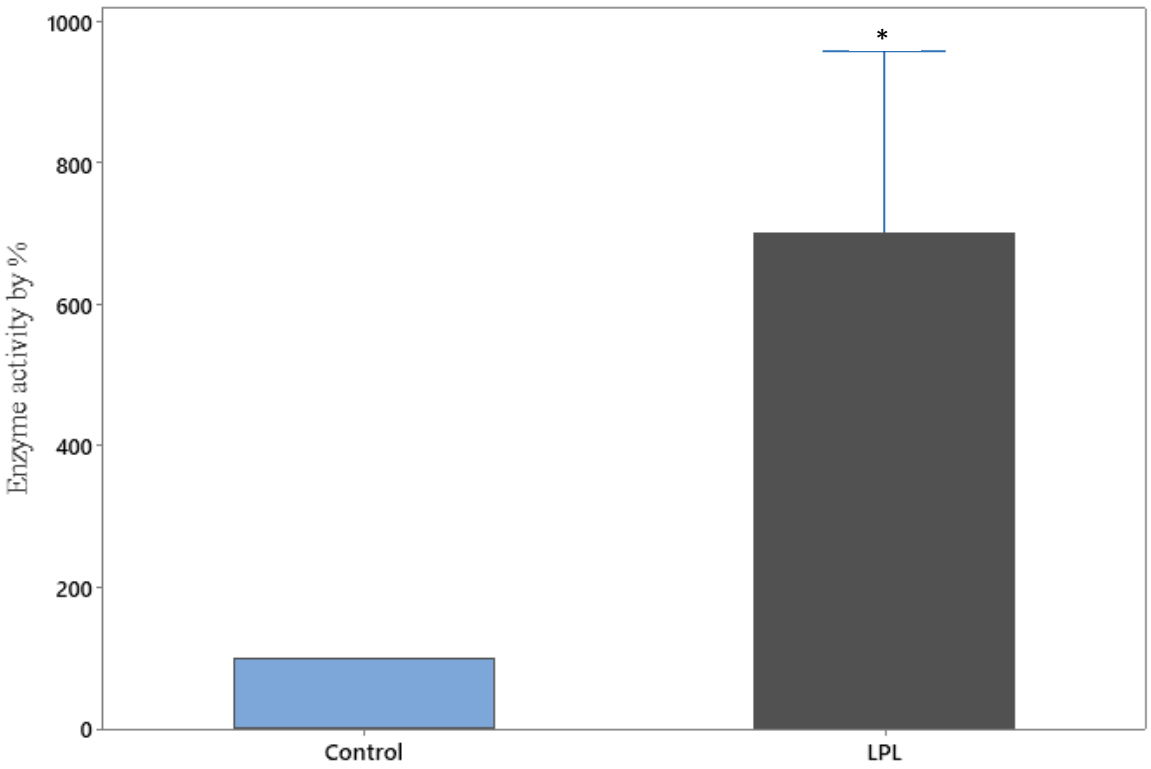
1000
800
600
400
200
0
Enzyme activity by %
*
Control
LPL

Figure 7: Protein expression and enzymatic activity of LPL.

HEK-293 cells were transfected with the pcDNA3 vector without or with the human LPL cDNA. The heparinized media of each sample were collected, as described in section 2.1.3. (A) Western blot analysis of the heparinized media from cells transfected with pcDNA3-hLPL showed expression of LPL by the cells, and no LPL expression in the heparinized (control) media from cells transfected with empty vector pcDNA3. (B) Lipase activity of heparinized media from cells transfected with pcDNA3 (control) or pcDNA3-hLPL, using a resorufin ester substrate assay, as described in section 2.2.2 (Figure generated using Minitab). The control enzyme activity was normalized to 100%, and data are presented as percent of control and mean ± SD for biological replicates, n=3. *, p=0.039.

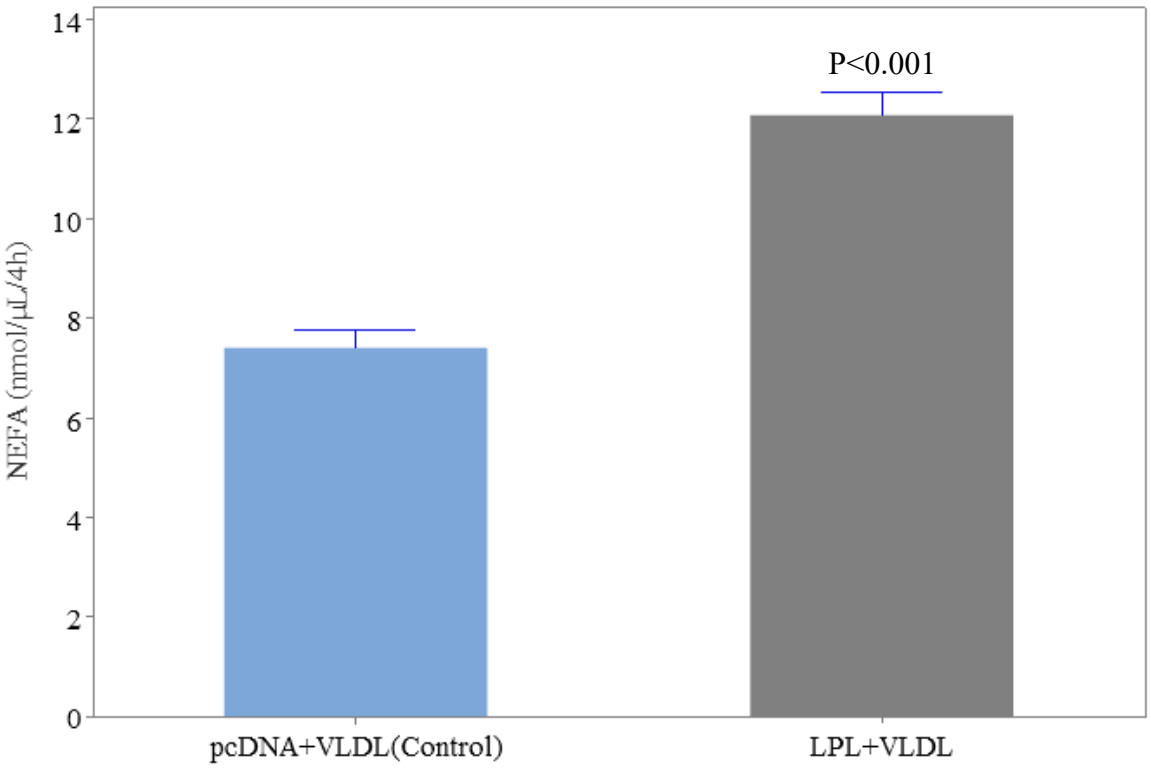

Figure 8: Non-esterified fatty acid (NEFA) assay of VLDL hydrolysis products by LPL.

Heparinized media collected from cells expressing LPL, or control-transfected cells, were incubated with VLDL (with total cholesterol = 5,300 mg/dL & triglyceride = 14,120 mg/dL) for 4 hours. The concentration of NEFA in the generated hydrolysis products was quantified. Data are presented as mean ± SD of NEFA concentration for biological replicates n=3. p<0.001. Figure generated using Minitab.

3.2 Effect of VLDL HPs by LPL with or without NOXi on the ROS production in THP-1 macrophages

To evaluate the effect of VLDL HPs by LPL on ROS production in THP-1 macrophages in the absence or presence of NOXi, VLDL HPs produced by LPL were diluted to an FFA concentration of 0.25 mM. The diluted VLDL HPs were then incubated with macrophages for 18 hours with or without either 100 μM of apocynin or 20 μM of GKT136901, as described in section 2.3.6. The VLDL HPs generated by heparinized media from control cells were diluted to mimic the diluted VLDL HPs by LPL, which yielded an approximate FFA concentration of 0.15 mM; these and 100 μM TBHP were the negative control and positive control samples, respectively. The control samples were incubated with THP-1 macrophages for 18 hours (as described in section 2.3.6). The cells treated with 0.25 mM FFA from VLDL HPs by LPL generated ROS values that were significantly higher ($(2.12 \pm 0.36) \times 10^4$ a.u and $(2.01 \pm 0.28) \times 10^4$ a.u) than the ROS values generated by the control VLDL HPs ($(9.35 \pm 2.22) \times 10^3$ a.u and $(9.26 \pm 1.61) \times 10^3$ a.u) (Figures 9 and 10 respectively). Macrophages treated with 0.25 mM FFA of VLDL HPs and 100 μM of apocynin showed no significant difference when compared to the cells treated with 0.25 mM FFA from VLDL HPs by LPL without apocynin (Figure 9). Macrophages treated with 0.25 mM FFA from VLDL HPs by LPL and 20 μM of GKT136901 showed a significant decrease in ROS generated compared to cells treated with 0.25 mM FFA from VLDL HPs by LPL without GKT136901 (Figure 10).

Figure 9

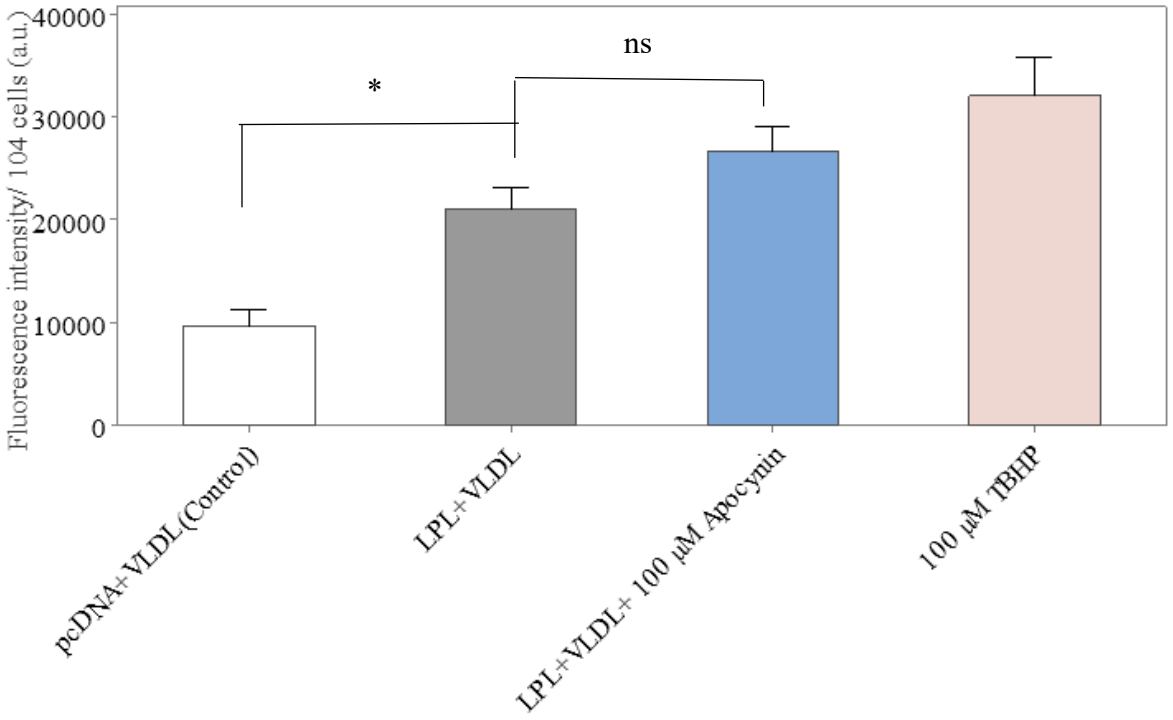

Figure 9: Apocynin did not inhibit ROS production in VLDL hydrolysis product-treated macrophages.

THP-1 macrophages were treated with 0.25 mM (by FFA) VLDL hydrolysis products by LPL with or without 100 µM apocynin, pcDNA3 (control), or 100 µM TBHP (positive control) for 4 hours. ROS production was measured by fluorescence intensity per 10^4 cells using the DCFDA cellular assay. Bars represent mean ± SD of fluorescence intensity per 10^4 cells for biological replicates, n=3. *, p<0.05. Figure generated using Minitab.

Figure 10

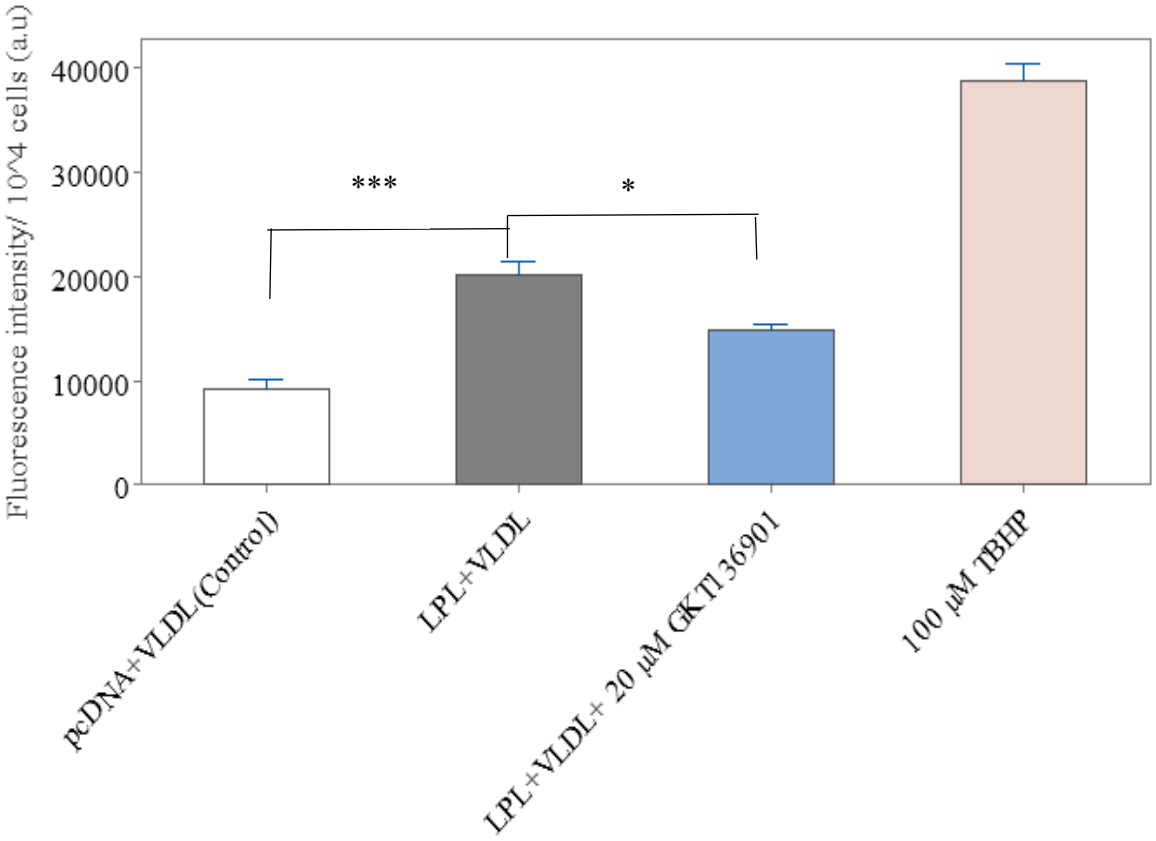

Figure 10: GKT136901 inhibits ROS production in VLDL hydrolysis product-treated macrophages.

THP-1 macrophages were treated with 0.25 mM (by FFA) VLDL hydrolysis products by LPL with or without 20 µM GKT136901, pcDNA3 (control), or 100 µM TBHP (positive control) for 4 hours. Fluorescence intensity per 10^4 cells was measured using DCFDA cellular assay. Bars represent mean ± SD of fluorescence intensity per 10^4 cells for biological replicates, n=4. *, $p<0.05$, and ***, $p<0.001$. Figure generated using Minitab.

3.3. Effect of VLDL HPs by LPL with or without GKT136901 on lipid peroxidation of THP-1 macrophages

Lipid peroxidation in THP-1 macrophages treated with VLDL HPs by LPL was assessed due to the significant increase in ROS generated in VLDL HPs by LPL-treated macrophages compared to ROS generated in VLDL HPs by control-treated macrophages. The formation of lipid peroxides in macrophages was determined by measuring MDA levels using a TBARS assay, as described in section 2.4.2. Both intracellular and extracellular MDA levels in the macrophages were assessed by measuring the TBARS concentration in both media and cell lysates. The macrophages were treated with or without 20 μM of GKT136901, and positive control cells were treated with 100 μM TBHP. There was no significant difference in TBARS concentration in macrophages across all treatment and control groups in both media and cell lysates (Figures 11A and 11B). Thus, the effect of VLDL HPs by LPL with or without GKT136901 on ROS levels did not affect MDA levels in treated macrophages.

Figure 11

A.

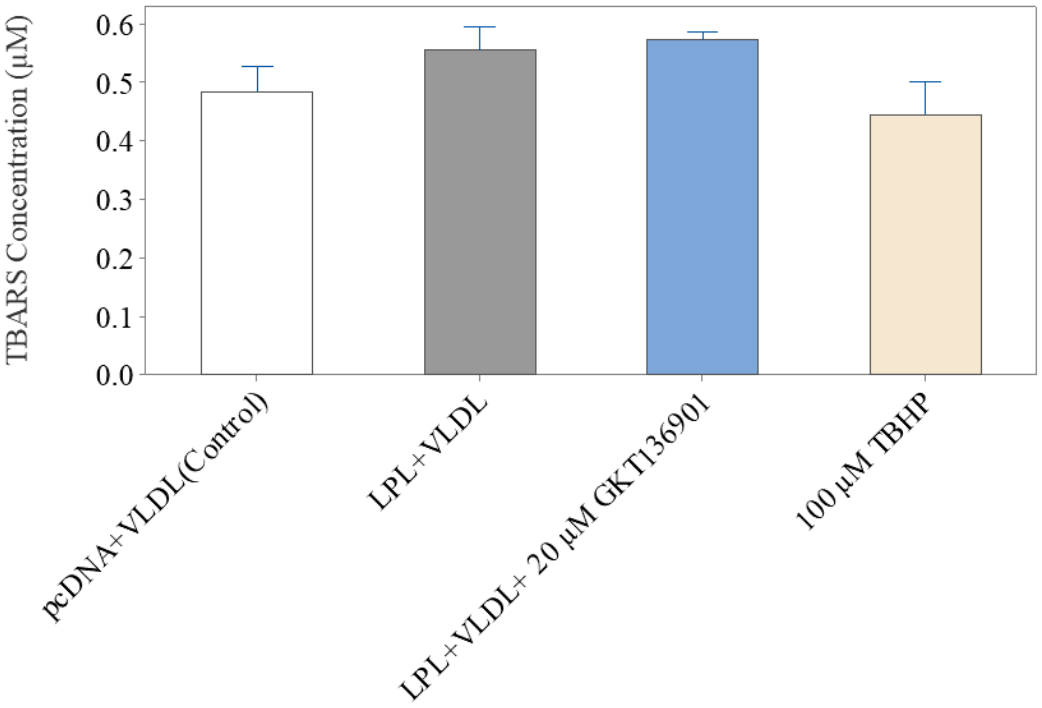
TBARS Concentration (µM)
0.0
0.1
0.2
0.3
0.4
0.5
0.6
pcDNA+VLDL(Control)
LPL+VLDL
LPL+VLDL+ 20 µM GKT136901
100 µM TBHP

B.

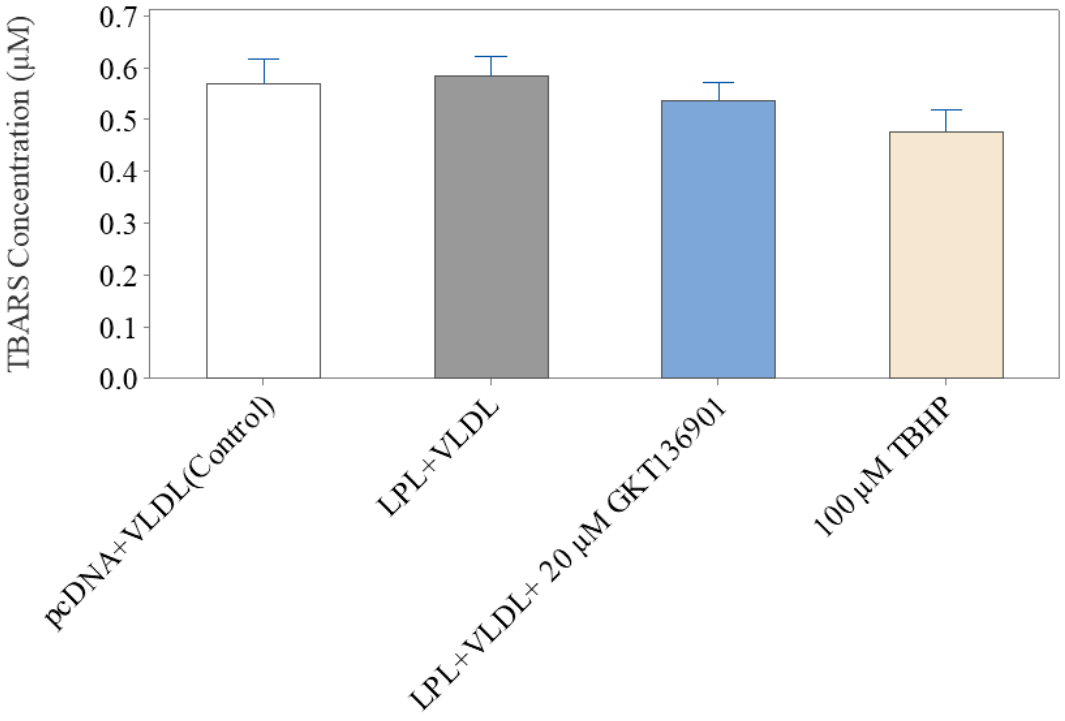
TBARS Concentration (µM)
0.0
0.1
0.2
0.3
0.4
0.5
0.6
0.7
pcDNA+VLDL(Control)
LPL+VLDL
LPL+VLDL+ 20 µM GKT136901
100 µM TBHP

Figure 11: VLDL hydrolysis products by LPL with or without 20 μM GKT136901 did not induce lipid peroxidation in macrophages.

THP-1 macrophages were treated with 0.25 mM (by FFA) VLDL hydrolysis products by LPL with or without 20 μM GKT136901, pcDNA3 (control), or 100 μM TBHP (positive control) for 18 hours. (A) Thiobarbituric acid reactive substance/malondialdehyde (TBARS/MDA) concentration in the cell lysate of 10^6 treated cells was measured. (B) TBARS/MDA concentration in the cell culture media of 10^6 treated cells was measured. Bars represent mean ± SD of TBARS/MDA concentration per 10^6 cells for biological replicates, n=3. Figure generated using Minitab.

3.4 Effect of VLDL HPs by LPL on RNA quality in macrophages

Total RNA samples were isolated from THP-1 macrophages treated with VLDL HPs by LPL for 18 hours with or without 20 μM of GKT136901, as described in section 2.5, for RNA quality analyses. Macrophages were incubated with VLDL HPs generated by the heparinized media from control cells, and 100 μM TBHP, as control and positive control groups, respectively. The 1% agarose gel image of the total RNA samples after DNase treatment showed no significant difference in the levels of both 28S and 18S ribosomal RNA in response to VLDL HPs by LPL (Figure 12A). The RNA integrity number from all the samples was above nine, with no significant difference across all treatment and control groups (Figure 12B). Thus, 0.25 mM (by FFA) VLDL HPs by LPL with or without 20 μM of GKT136901 has no effect on RNA quality.

3.5 Expression of *SNORA56*, *SNORA60*, and *SNORA80E* in macrophages treated with VLDL HPs by LPL by Real-Time PCR

Our laboratory previously carried out microarray analyses of the total RNA isolated from THP-1 macrophages incubated in the absence or presence of total lipoprotein HPs generated by LPL, and it was seen that 63 of all upregulated transcripts were snoRNAs (89), with *SNORA56*, *SNORA60*, and *SNORA80E* being part of the prominent snoRNAs upregulated.

I chose to assess the expression of *SNORA56*, *SNORA60*, and *SNORA80E* in THP-1 macrophages treated with VLDL HPs by LPL for 18 hours using real-time PCR, as described in section 2.5.3, to build on the above microarray data. In this present study, there was no significant difference in the expression of *SNORA56*, *SNORA60*, and *SNORA80E* in

macrophages treated with VLDL HPs by LPL with or without 20 μM of GKT136901 compared to the control group (Figure 13A, B,& C). Only the TBHP-treated macrophages showed a significantly decreased expression of *SNORA56* (Figure 13A).

Figure 12

A.

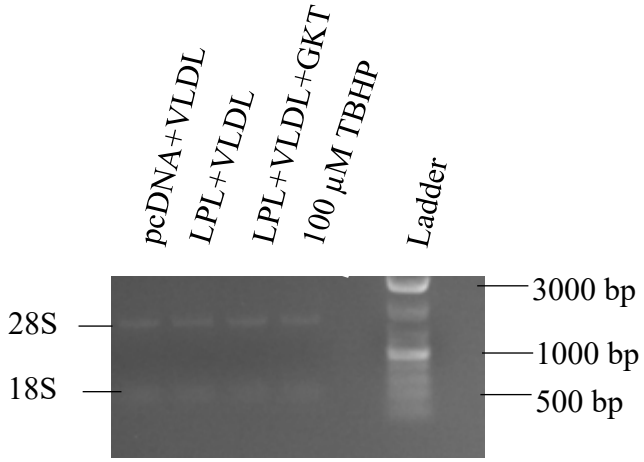
pcDNA+VLDL
LPL+VLDL
LPL+VLDL+GKT
100 μM TBHP
Ladder
28S
18S
3000 bp
1000 bp
500 bp

B.

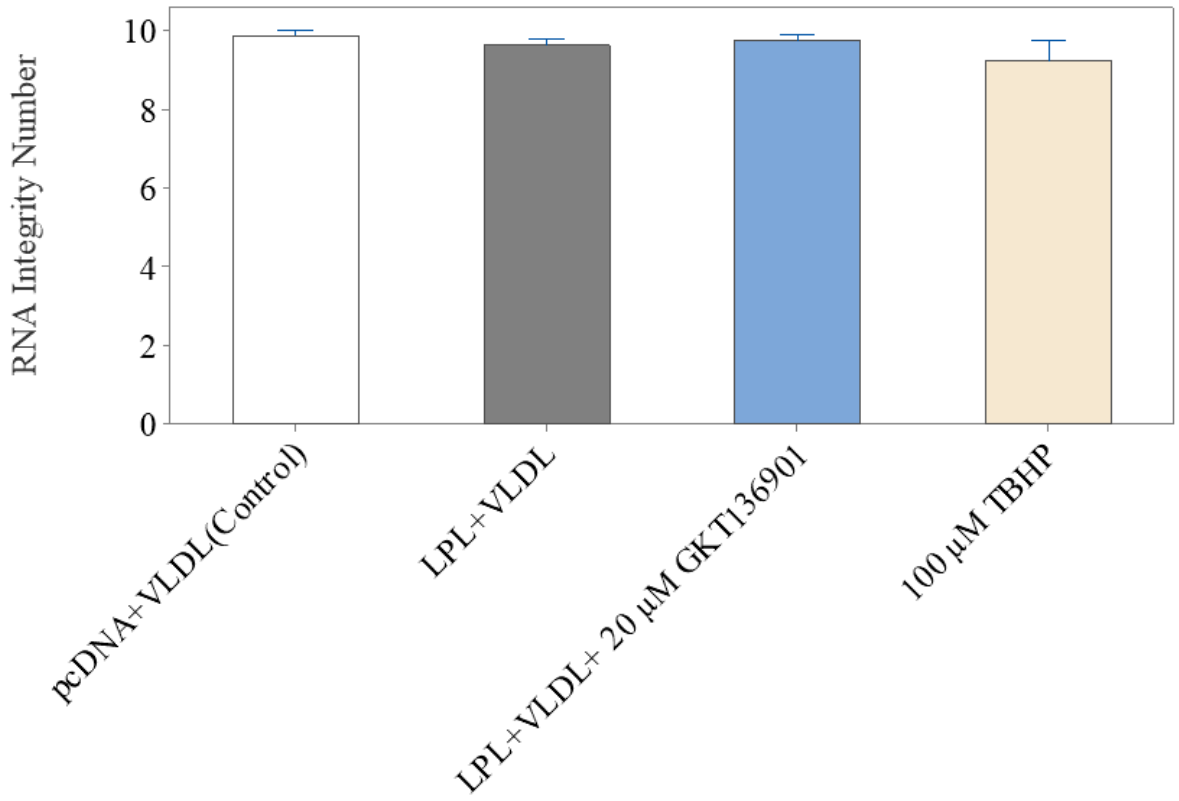
RNA Integrity Number
10
8
6
4
2
0
pcDNA+VLDL(Control)
LPL+VLDL
LPL+VLDL+ 20 μM GKT136901
100 μM TBHP

Figure 12: VLDL hydrolysis products by LPL with or without 20 μM GKT136901 show no effect on RNA quality in treated macrophages.

THP-1 macrophages were treated with 0.25 mM (by FFA) VLDL hydrolysis products by LPL with or without 20 μM GKT136901, pcDNA3 (control), or 100 μM TBHP (positive control) for 18 hours, and total RNA was isolated. (A) 1% Agarose gel showing 28S and 18S rRNA bands of total RNA isolated. (B) A graphical presentation of the RNA integrity number of total RNA isolated from treated macrophages. Data are presented as mean ± SD for biological replicates, *n*=5. Figure generated using Minitab.

Figure 13

A.

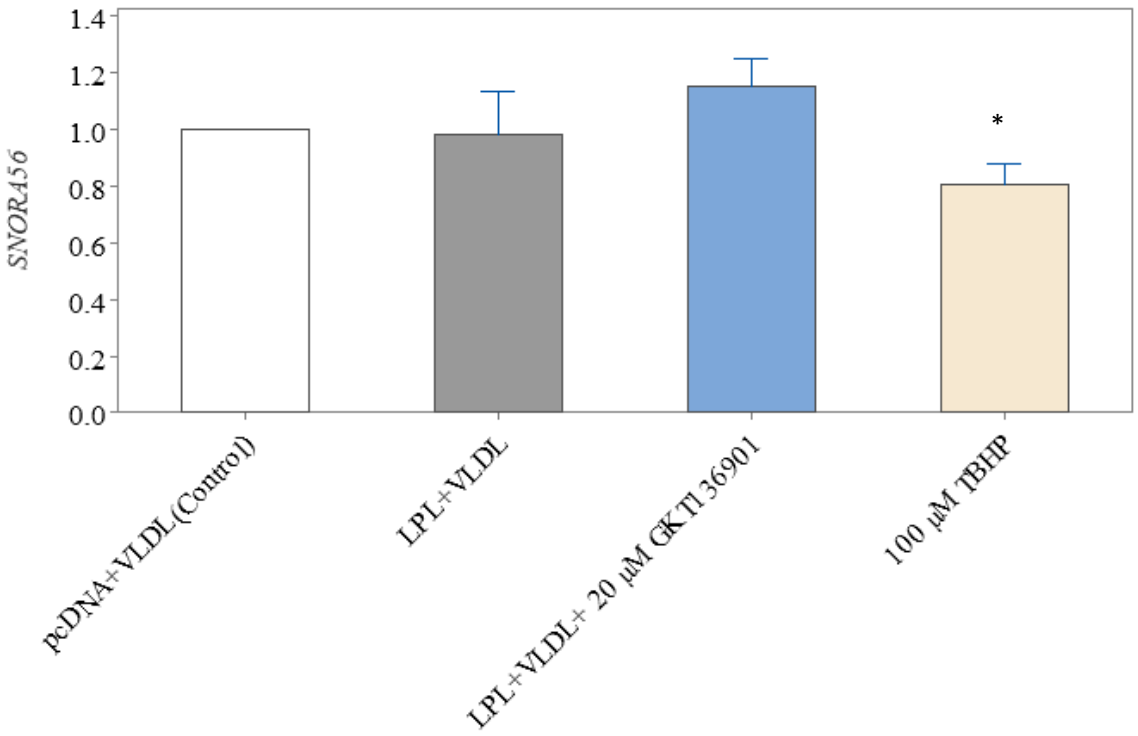
SNOR456
1.4
1.2
1.0
0.8
0.6
0.4
0.2
0.0
*
pcDNA+VLDL(Control)
LPL+VLDL
LPL+VLDL+ 20 μM GKT136901
100 μM TBHP

B.

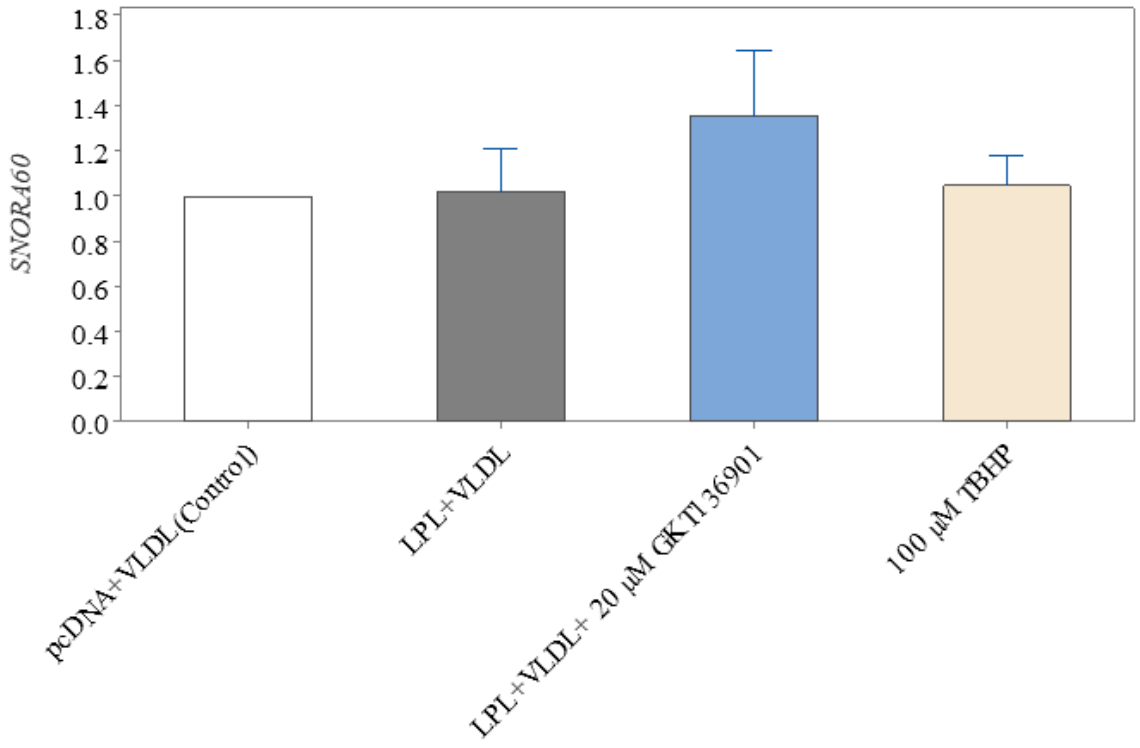
SNOR460
1.8
1.6
1.4
1.2
1.0
0.8
0.6
0.4
0.2
0.0
PcDNA+VLDL (Control)
LPL+VLDL
LPL+VLDL+ 20 μM GKTI 36901
100 μM TBHP

C.

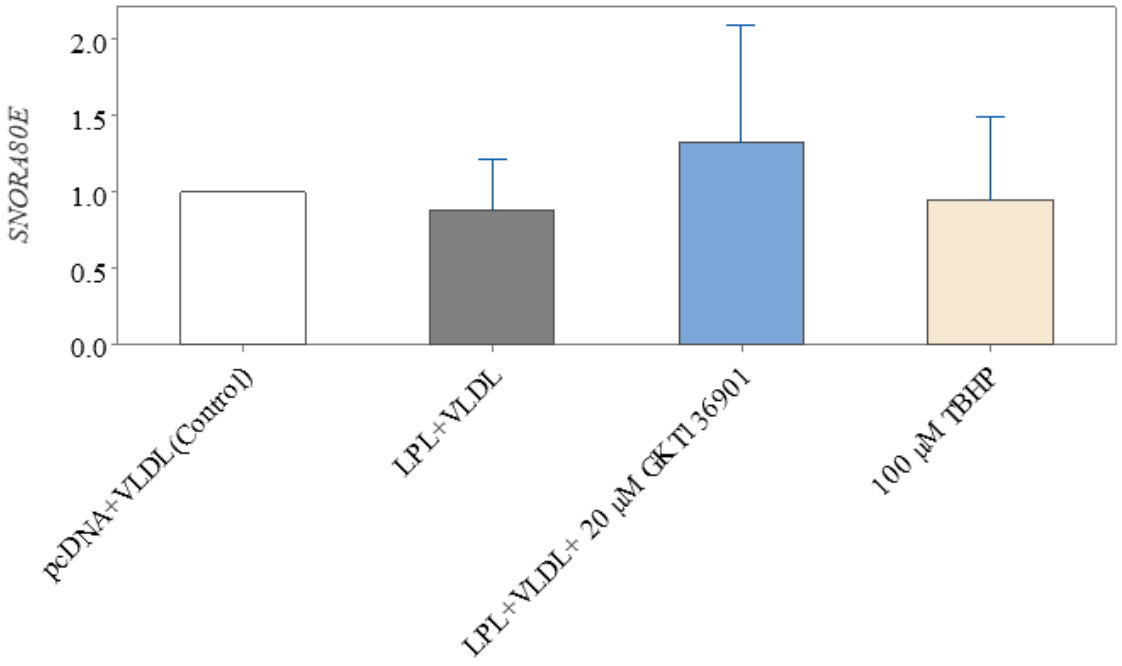

Figure 13: Small nucleolar RNA expression analysis in THP-1 macrophages treated with VLDL hydrolysis products by LPL with or without 20 µM GKT136901.

THP-1 macrophages were treated with 0.25 mM (by FFA) VLDL hydrolysis products by LPL with or without 20 µM GKT136901, pcDNA3 (control), or 100 µM TBHP (positive control) for 18 hours. Total RNA was isolated, and qPCR was carried out. Fold change, normalized to *ACTB*, was quantified for (A) *SNORA56*, (B) *SNORA60*, and (C) *SNORA80E*. Bars represent mean ± SD for biological replicates, n=3 (A and B) and n=4 (C). *, p<0.05. Figure generated using Minitab.

CHAPTER 4: DISCUSSION

4.1 Elevated FFAs may contribute to the increase in ROS production and macrophage function regulation in atherosclerosis

In this study, I incubated THP-1 macrophages with VLDL HPs generated by LPL. Oxidative stress in macrophages, which results from an increase in the production of ROS and impaired antioxidant defenses, contributes to endothelial dysfunction observed in atherosclerosis. This study demonstrated that exposure of THP-1 macrophages to VLDL HPs generated by LPL induced a significant increase in ROS production in macrophages. A similar observation was seen in a previous study, where human aortic endothelial cells (HAECs) were treated with TGRL and LPL (93). A previous study demonstrated a significant increase in ROS production in HAECs treated with VLDL lipolysis FFA assessed DCFDA oxidation (93). The prior study also showed a significant decrease in ROS production induced by FFA In HAECs in the presence of NOXi (93).

As expected, this study established that VLDL HPs generated by LPL increase ROS generation significantly in macrophages. This increase may be due to the activation of NOX by VLDL HPs in the macrophages. NOX is known to be activated through complex mechanisms, including protein-protein interaction of subunits (97,98), phosphorylation of cytosolic subunits (97), small GTPases (98,99), calcium and EF-hand domains binding (98), and lipid signaling (99,100,101), with the specific activation pathways varying between NOX isoforms.

PIP_2 aids in the translocation of NOX5 from internal membranes to the plasma membrane by binding to the N-terminal polybasic region of NOX5 (105). This localization of NOX5 to the plasma membrane is important for producing extracellular ROS. Membrane PIP_2 and PIP_3 are

preferentially targeted by the PX domain of NOXO1, a NOX1 organizer subunit and a homolog of p47phox, to facilitate the assembly and activation of NOX1 (102,103). PIP_2 and PIP_3 participate in regulating protein kinase C (PKC) activity. PKC, an important activator of NOX enzymes, phosphorylates regulatory subunits like p47phox, which is important for NOX2 activation. Another lipid that has been reported to promote superoxide production is arachidonic acid. Arachidonic acid induces conformational changes in cytosolic NOX subunits by directly releasing the p47phox SH3 domains from the autoinhibition region and enabling their interaction with p22phox of the flavocytochrome b558 transmembrane complex (106). Arachidonic acid activates NOX indirectly by inducing signaling molecules like PKC (107). Upon the significant increase in ROS production in macrophages incubated with VLDL HPs by LPL, this study further investigated if NOX is the mediator of the increase in ROS production seen in VLDL HPs by LPL-treated macrophages. This was done by treating the macrophages with VLDL HPs by LPL with or without NOX inhibitors. The next section shows that NOX mediates the increase in ROS production in macrophages using GKT136901.

4.2 GKT136901 inhibits ROS production in THP-1 macrophages, while apocynin does not affect ROS production

In this study, while apocynin showed no inhibitory activity against NOX, GKT136901, on the other hand, exhibited inhibitory activity against NOX in PMA-differentiated macrophages. Apocynin is a widely known inhibitor of NOX enzymes, but its mode of action and effects are complex and controversial. Prior studies have been carried out in several cell types, including endothelial cells and multipotent mesenchymal stem cells, where apocynin has been seen to exhibit inhibitory effect against NOX (108,109,110). Apocynin, a natural methoxy-

substituted catechol isolated from *Picrorhiza kurroa* (111), prevents the translocation of cytosolic subunits (p47phox, p67phox, and p40phox) to the membrane, thereby inhibiting the assembly of an active NOX complex at the plasma or organelle membrane (112). Apocynin has been shown to inhibit the production of superoxide ions *in vitro* (108) and to exhibit both anti-oxidative and anti-inflammatory effects *in vivo*.

Apocynin exhibited inhibitory effects on advanced glycation end-products-induced oxidative stress by downregulating the gene expression of NOX-1, NOX-4, and IL-6 and reducing ROS induction in rotator cuff-derived cells (108). Apocynin showed inhibitory effects against NOX activity in rats by lowering plasma F2-isoprostane concentrations in adrenocorticotropic hormone-induced hypertension (109) and by decreasing lipopolysaccharide-induced NOX-derived ROS production in lung homogenates of lipopolysaccharide-administered rats (110). Although apocynin attenuated FFA-induced ROS production in HAECs (93), in this study, apocynin did not attenuate VLDL HP-induced ROS production within THP-1 macrophages. The failure of apocynin to inhibit VLDL HP-induced ROS production within THP-1 macrophages in this study may be a result of the absence or less activity of myeloperoxidase (MPO) in macrophages. Apocynin requires activation by MPO in the presence of H_2O_2 to form a reactive dimer, diapocynin, that can bind to cysteine residues on p47phox, thus inhibiting NOX activity (113,114). THP-1 macrophages are reported to exhibit little or no MPO expression compared to neutrophils (115). Interestingly, a prior study showed that the inhibitory activity of apocynin in neutrophils stimulated with opsonized zymosan was significantly higher than that of neutrophils stimulated with PMA, with IC50 values of 10 μM and 1500 μM, respectively (116). This further indicates that PMA-stimulated macrophages may have less active MPOs or MPOs with no measurable enzyme activity (Brown 2019, unpublished), which hinders the formation of

diapocynin, the active apocynin dimer, thus lowering the inhibitory activity of apocynin in these cells. This shows that the effect of apocynin can vary widely depending on the experimental system and conditions used.

GKT136901, on the other hand, showed significant inhibitory activity against NOX in PMA-stimulated THP-1 macrophages. GKT136901 (2-(2-chlorophenyl)-4-methyl-5-(pyridin-2-ylmethyl)-1H-pyrazolo [4,3-c]pyridine-3,5(2H,5H)-dione), a pyrazolopyridine derivative, is a selective NOX1 and NOX4 inhibitor that was developed after high-throughput screening and structure-activity relationship investigation (117). GKT136901 exhibited high potency for inhibiting NOX4 and NOX1, with K_i of 165 ± 5 nM and 160 ± 10 nM, respectively. GKT136901 inhibited NOX5 with a K_i of about 450 nM and showed approximately 10-fold selectivity for NOX1/4 over NOX2, with a K_i of 1530 ± 90 nM for NOX2. GKT136901, in this present study, demonstrates NOX1/4 involvement in atherosclerosis. Previous studies have demonstrated NOX1/4 involvement in various diseased conditions, including diabetic nephropathy (118) and methamphetamine (METH)-induced cerebrovascular dysfunction (119). In diabetic mice, GKT136901 was renoprotective through reduced lipid peroxidation (118). GKT136901 also inhibited METH-induced ROS generation in primary human brain microvascular endothelial cells after 24 hours METH exposure (119). The molecular mechanism of action that GKT136901 utilizes to carry out its inhibitory effect on NOX 1/4 and ROS production is still unclear.

Some previous studies have, however, called into question the mechanism of action of GKT136901 as a NOX inhibitor. While one study found that GKT136901 acts as a selective scavenger of peroxynitrite (120), another study showed that GKT136901 interferes with peroxidase-dependent assays used to measure NOX activity rather than a direct NOX inhibitor (121). Further research should be carried out to fully characterize the inhibitory effects and

mechanism of action of GKT136901 on NOX enzymes. Overall, this present study's data show the activity NOX1/4 in ROS production and its inhibition by GKT136901 in PMA-differentiated THP-1 macrophages using a DCFDA assay.

4.3 NOX-mediated ROS did not induce lipid peroxidation in THP-1 macrophages treated with VLDL HPs with low FA concentration

Lipid peroxidation is an important player in the development and progression of atherosclerosis. Lipids become atherogenic when oxidized by ROS produced by cells, which include endothelial cells, smooth muscle cells, and macrophages, in the artery wall (122). Oxidized lipids contribute to the inflammation and oxidative stress seen in atherosclerosis by activating inflammatory pathways and increasing the expression of pro-inflammatory cytokines like TNF-α and IL-1β (123). In this study, I investigated how the increase in ROS production observed in THP-1 macrophages treated with VLDL HPs generated by LPL affects lipid peroxidation intracellularly and extracellularly. As mentioned earlier, macrophages produce ROS through NOX enzymes at the cell membrane, as well as through the mitochondrial electron transport chain and other oxidases. The ROS produced initiates lipid peroxidation by abstracting hydrogen atoms from PUFAs and membrane lipoproteins, thereby creating lipid radicals (124). The lipid radicals formed react with O_2 to form lipid peroxy radicals, which in turn abstracts hydrogen from other lipids, resulting in a chain reaction. This chain reaction can be terminated when antioxidants donate hydrogen atoms to the lipid peroxy radicals (124). A common lipoprotein particle usually oxidized in the artery wall during atherosclerosis development is LDL. Ox-LDLs are typically formed through the oxidation of LDL particles by ROS produced

by macrophages. Uptake and accumulation of ox-LDL via macrophage scavenger receptors leads to the transformation of macrophages into foam cells (123).

Lipid hydroperoxides formed during lipid peroxidation are usually broken down into reactive aldehydes such as 4-hydroxynonenal (4-HNE) and malondialdehyde (MDA). These aldehydes mediate the transduction of cell signals and regulation of gene expression and can cause cell damage through protein and DNA modifications. MDA is a standard indicator of lipid peroxidation, and a significant increase in its level has been observed in hypertensive and atherosclerotic animal models (125, 126,127). In this study, MDA was quantified spectrophotometrically upon its reaction with thiobarbituric acid, which gives a fluorescent red derivative. This study observed no significant increase in lipid peroxidation in THP-1 macrophages treated with VLDL HPs compared to control. This may be due to the concentration of lipids, which includes triglycerides (114.58 mg/dL), total cholesterol (43.01 mg/dL), and free fatty acids (0.25 mM), in the VLDL HPs by LPL treatment media being within the normal and low-risk range (141). Normolipidemic subjects, in prior studies (128,129), have been seen to exhibit lower MDA plasma concentrations compared to hyperlipidemic subjects.

4.4 NOX-mediated ROS did not induce alterations in *SNORA56*, *SNORA60*, and *SNORA80E* expression in THP-1 macrophages treated with VLDL HPs with low FA concentration

In this study, I isolated total RNA from THP-1 macrophages treated with VLDL HPs in the absence or presence of GKT136901. The RNA quality and RNA integrity number (RIN) were assessed, with no significant difference between the RIN of the control and treatment groups. The isolated RNAs were highly intact, with all groups having RINs above 9. These high-quality,

intact RNAs were necessary for accurate gene expression analysis. The analysis of gene expression patterns in atherosclerosis aids in gaining a comprehensive understanding of the disease process, identifying new biomarkers for detection and disease outcome, and developing targeted therapies to prevent or treat this complex cardiovascular disease.

Various gene expression patterns are observed in cellular processes crucial to atherosclerosis development. These include the significant overexpression of pro-inflammatory cytokine genes, *TNFA* (encoding TNF-α) and *IL1B* (encoding IL-1β) (130), overexpression of triggering receptors expressed on myeloid cells (TREMs) in inflammatory lipid-associated macrophages associated with symptomatic atherosclerosis (131), and differential expression of *ABCA1*, *ABCG1*, *APOE*, and *PLIN2* involved in lipid metabolism (131,132). These gene expression patterns contribute to the complicated cellular environment and foam cell formation, including modified LDL uptake, cholesterol efflux, lipid metabolism, and inflammatory responses observed in macrophages found within atherosclerotic plaques.

A previous study in our laboratory investigated gene expression patterns in THP-1 macrophages treated with total lipoprotein hydrolysis products by LPL using microarray analyses and observed upregulation of *CD36*, *PLIN2*, *FABP4*, and *CPTIA*. At the same time, *ACAT2*, *FASN*, *FADS1*, *FADS2*, and *LDLR* were downregulated (89). Interestingly, 63 out of the 183 upregulated transcripts in our prior study were snoRNAs. The crucial roles of snoRNAs and their overexpression in THP-1 macrophages treated with lipoprotein HPs generated by LPL, as observed by Thyagarajan *et al*. (89), provided the rationale for the investigation of NOX-induced ROS production as a mediator of snoRNA overexpression in THP-1 macrophages treated with VLDL HPs generated by LPL in this present study. I chose to investigate the expression of *SNORA56*, *SNORA60*, and *SNORA80E* in THP-1 macrophages treated with VLDL HPs because

these snoRNAs are among the 14 snoRNAs out of the 63 upregulated snoRNAs that were identified to exhibit a fold change greater or equal to four in response to total lipoprotein HPs (89). All three snoRNAs are H/ACA box snoRNAs, with their primary function being to guide the pseudouridylation of RNAs. *SNORA56* guides the pseudouridylation of 28S rRNAs at U1664, and it is found embedded in an intron of the *DKC1* - dyskerin gene, while *SNORA60* guides the pseudouridylation of 18S rRNAs at U1004, and it is found embedded in an intron of the *SNHG11* gene (137). *SNORA80E*, known as *SNORA42*, is embedded in *KIAA0907* and guides the pseudouridylation of 18S rRNA at U572 and U109 (137). While emerging specific functions of *SNORA60* and *SNORA80E* are not yet reported, *SNORA56* has been reported to be overly expressed in colorectal cancer tissues and plasma and promote the translation of glutamate-cysteine ligase catalytic subunit (GCLC), a major enzyme in glutathione biosynthesis (138). Glutathione, a known antioxidant, suppresses lipid peroxidation. Overly expressed *SNORA56* causes glutathione synthesis, thus inhibiting iron-dependent apoptosis in cells (138). In this present study, there was no significant alteration in the expression of *SNORA56* in macrophages treated with VLDL HPs compared to control. The gene response within VLDL HP-treated macrophages may result from NOX-induced ROS formation being inadequate to induce lipid peroxidation in macrophages treated with VLDL HPs within the normal and low-risk range. In contrast to this observation, as reported by Thyagarajan *et al.* (89), upregulation of *SNORA56* was seen in macrophages treated with total lipoprotein HPs by LPL with FFA content of 0.68 mM. This suggests that a high concentration of lipids will induce oxidative stress in macrophages, which will, in turn, upregulate the expression of *SNORA56*. Therefore, I can presumably hypothesize that macrophages employ the overexpression of *SNORA56* and its product to regulate the cell's antioxidant capacity, lipid metabolism, and survival of foam cells

through glutathione synthesis in atherosclerosis. No significant alteration in the expression of both *SNORA60* and *SNORA80E* by NOX-induced ROS with or without GKT136901 was observed in this study. This may be associated with the low lipid peroxidation observed in the treated macrophages with or without GKT136901. Although the specific functions of *SNORA60* and *SNORA80E* in macrophages are still unclear, high expression levels of both snoRNAs have been reported in cancer cells. This suggests that overexpression of *SNORA60* and *SNORA80E* is a response to cell oxidative stress. The difference in gene response observed in macrophages treated with HPs by LPL in this present study and the laboratory's prior study by Thyagarajan *et al*. may be due to the different hydrolysis products used in treating the macrophages in both studies. While Thyagarajan *et al*. used total lipoprotein HPs with constituents from all lipoprotein classes, which include the highly lipotoxic Lp(a) and LDL, this present study treated the macrophages with VLDL HPs containing constituents specific to VLDL particles. This speculation is further buttressed by the varied modulation of *SNORA56* expression demonstrated by macrophages treated with the various components of the total lipoprotein HPs used in Thyagarajan's study, where total lipoprotein HPs upregulated *SNORA56* expression, saturated fatty acids downregulated *SNORA56* expression, and total FFA did not affect *SNORA56* expression (89). The overall data from this study show that NOX-mediated ROS did not induce overexpression of *SNORA56, SNORA60,* and *SNORA80E* due to low lipid peroxidation in macrophages treated with VLDL HPs by LPL within the normolipidemic range with or without GKT136901.

4.5 Study limitations

PMA is commonly used to differentiate THP-1 monocytes into macrophages, leading to increased expression of NADPH oxidase components, specifically, p47phox (13). Apocynin inhibits NOX by preventing the translocation of p47phox to the membrane. To carry out its inhibitory function, apocynin is oxidized by MPO and condensed to form an active dimer, diapocynin. PMA-differentiated macrophages have been reported to have significantly lower levels of MPO compared to monocytes or neutrophils (115), which result in apocynin's inactivity in these cells. The inability of apocynin to inhibit ROS production in this present study may lead to an incorrect conclusion that NOX is not the mediator of ROS production in macrophages treated with VLDL HPs generated by LPL. This limitation was addressed by using a different inhibitor, GKT136901.

The use of THP-1 monocyte-derived macrophages instead of primary human monocyte-derived macrophages is another limitation in this study. THP-1 monocyte-derived macrophages are known to show less pronounced changes in target gene expression and differences in response to activating stimuli compared to primary human monocyte-derived macrophages (142). Furthermore, my study used only 0.25 mM (by FFA) of VLDL HPs. This would represent a normal FFA profile rather than a hyperlipidemic profile seen in atherosclerosis. The ROS produced by this low lipid concentration seems not to induce cellular damage.

4.6 Future research directions

To further validate the role of NOX in ROS production in PMA-differentiated macrophages treated with VLDL HPs generated by LPL, diapocynin, the active dimer of apocynin, should be used as a NOXi.

This study shows that ROS production induced by NOX did not mediate lipid peroxidation and snoRNA overexpression within THP-1 macrophages treated with VLDL HPs containing low/normal concentrations of lipids. Therefore, research where macrophages are treated with VLDL HPs with FFA content of 0.75 – 1 mM should be carried out representing high lipid levels seen in atherosclerosis. This further study should assess lipid peroxidation and snoRNA expression at different time points to clarify the sequence order of both occurrences.

Further investigation of the expression of Nrf2 pathway genes in macrophages treated with lipoprotein HPs by LPL will provide insight into how the macrophages were able to prevent lipid peroxidation in the presence of significantly increased NOX-induced ROS. This investigation will also elucidate new emerging functions of snoRNAs and their possible interaction with the Nrf2 transcription factor in macrophages' cellular redox balance. In the future study, the effect of NOX-induced ROS on lipid peroxidation and expression of snoRNAs and Nrf2 pathway genes, like *GCLC*, *GCLM*, and *GPX1*, in macrophages treated with either low/normal or high concentrations of lipids will be evaluated.

4.7 Overall conclusions

This study has shown that VLDL HPs generated by LPL mediate an increase in ROS production in THP-1 macrophages by activating NOX. My data show that GKT136901 inhibited

NOX-induced ROS production in PMA-differentiated THP-1 macrophages treated with VLDL HPs. At the same time, apocynin did not, possibly due to low expression or low activity of MPO in the THP-1 macrophages. The NOX-induced ROS production observed in the macrophages treated with VLDL HPs did not cause lipid peroxidation in the cells. This may be because the HPs' concentration is in the normolipidemic range, and the cells were able to maintain oxidative stress balance through their complex interplay of antioxidant systems. This study also showed that NOX-induced ROS in THP-1 macrophages treated with a physiological dose of VLDL HPs did not lead to the overexpression of *SNORA56, SNORA60,* and *SNORA80E* within the THP-1 macrophages.

References

1. Publications: Diseases and conditions; Heart Disease in Canada (2022, July 28). https://www.canada.ca/en/public-health/services/publications/diseases-conditions/heart-disease-canada.html
2. Moore, K.J., & Tabas, I. (2011)."Macrophages in the pathogenesis of atherosclerosis." *Cell* 145:341-355.
3. Xiang, P., Blanchard, V., & Francis, G.A. (2022). "Smooth muscle cell-macrophage interactions leading to foam cell formation in atherosclerosis: Location, location, location." *Front. Physiol*. 13:921597.
4. Botts, S.R., Fish, J.E., & Howe, K.L. (2021). "Dyslipidemia and endothelial dysfunction: A link to cardiovascular disease." *Front. Pharmacol*. 12:787541.
5. Gui, Y., Zheng, H., & Cao, R.Y. (2022). "The role of lipoproteins in cardiovascular disease: From mechanisms to clinical management." *Front. Cardiovasc. Med.* 9:845942.
6. Lusis, A.J. (2000). "Atherosclerosis." *Nature*, 407:233-241.
7. Navab, M., Berliner, J.A., Watson, A.D., Hama, S.Y., Territo, M.C., Lusis, A.J., Shih, D.M., Van Lenten, B.J., Frank, J.S., Demer, L.L., Edwards, P.A., & Fogelman, A.M. (1996). "The yin and yang of oxidation in the development of the fatty streak." *Arterioscler. Thromb. Vasc. Biol.* 16:831-842.
8. Vainio, S., & Ikonen, E. (2003). "Macrophage cholesterol transport: a critical player in foam cell formation." *Ann. Med.* 35:146-155.
9. Brown, M.S., & Goldstein, J.L. (1983). "Lipoprotein metabolism in the macrophage: Implications for cholesterol deposition in atherosclerosis." *Ann. Rev. Biochem.* 52:223-261.
10. Gimbrone Jr, M.A. (1999). "Vascular endothelium, hemodynamic forces, and atherogenesis." *Am. J. Pathol.* 155:1-5.
11. Borén, J., Olin, K., Lee, I., Chait, A., Wight, T.N., & Innerarity, T. L. (1998). "Identification of the principal proteoglycan-binding site in LDL. A single-point mutation in apo-B100 severely affects proteoglycan interaction without affecting LDL receptor binding."*J. Clin. Invest.* 101:2658-2664.
12. Goldstein, J.L., Ho, Y.K., Basu, S.K., & Brown, M.S. (1979). "Binding site on macrophages that mediates uptake and degradation of acetylated low density lipoprotein, producing massive cholesterol deposition." *Proc. Natl. Acad. Sci. U. S. A.* 76:333-337.
13. Dong, Z.M., Chapman, S.M., Brown, A.A., Frenette, P.S., Hynes, R.O., & Wagner, D.D. (1998). "The combined role of P- and E-selectins in atherosclerosis." *J. Clin. Invest.* 102:145-152.
14. Collins, R.G., Velji, R., Guevara, N.V., Hicks, M.J., Chan, L., & Beaudet, A.L. (2000). "P-Selectin or intercellular adhesion molecule (ICAM)-1 deficiency substantially protects against atherosclerosis in apolipoprotein E-deficient mice." *J. Exp. Med.* 191:189-194.
15. Smith, J.D., Trogan, E., Ginsberg, M., Grigaux, C., Tian, J., & Miyata, M. (1995). "Decreased atherosclerosis in mice deficient in both macrophage colony-stimulating factor (op) and apolipoprotein E." *Proc. Natl. Acad. Sci. U. S. A.* 92:8264-8268.
16. den Hartigh, L.J., Connolly-Rohrbach, J.E., Fore, S., Huser, T.R., & Rutledge, J.C. (2010). "Fatty acids from very low-density lipoprotein lipolysis products induce lipid droplet accumulation in human monocytes." *J. Immunol.* 184:3927–3936.
17. Kunjathoor, V.V., Febbraio, M., Podrez, E.A., Moore, K.J., Andersson, L., Koehn, S., Rhee, J.S., Silverstein, R., Hoff, H.F., & Freeman, M.W. (2002). "Scavenger receptors

class A-I/II and CD36 are the principal receptors responsible for the uptake of modified low density lipoprotein leading to lipid loading in macrophages." *J. Biol. Chem.* 277:49982-49988.
18. Tontonoz, P., Nagy, L., Alvarez, J.G., Thomazy, V.A., & Evans, R.M. (1998). "PPARγ promotes monocyte/macrophage differentiation and uptake of oxidized LDL." *Cell* 93:241-252.
19. Glass, C.K., & Witztum, J.L. (2001). "Atherosclerosis: The road ahead." *Cell* 104:503-516.
20. Ross, R. (1999). "Atherosclerosis — An inflammatory disease." *N. Engl. J. Med.* 340:115-126.
21. Berliner, J.A., Navab, M., Fogelman, A.M., Frank, J.S., Demer, L.L., Edwards, P.A., Watson, A.D., & Lusis, A.J. (1995). "Atherosclerosis: Basic mechanisms. Oxidation, inflammation, and genetics." *Circulation* 91:2488-2496.
22. Galis, Z.S., Sukhova, G.K., Lark, M.W., & Libby, P. (1994). "Increased expression of matrix metalloproteinases and matrix degrading activity in vulnerable regions of human atherosclerotic plaques." *J. Clin. Invest.* 94:2493-2503.
23. Moulton, K.S., Heller, E., Konerding, M.A., Flynn, E., Palinski, W., & Folkman, J. (1999). "Inhibition of plaque neovascularization reduces macrophage infiltration and atherosclerosis in apolipoprotein E-deficient mice." *Circulation* 99:1726-1732.
24. Davies, M.J., Richardson, P.D., Woolf, N., Katz, D.R., & Mann, J. (1993). "Risk of thrombosis in human atherosclerotic plaques: role of extracellular lipid, macrophage, and smooth muscle cell content." *Br. Heart J.* 69:377-381.
25. Lee, R.T., and Libby, P. (1997). "The unstable atheroma." *Arterioscler. Thromb. Vasc. Biol.* 17:1859-1867.
26. Schaffer, J.E. (2020). "Lipotoxicity: When tissues overeat." *J. Biol. Chem.* 295:8628-8635.
27. Watson H (2015). "Biological membranes." *Essays Biochem*. 59:43-69.
28. Feingold, K.R., & Grunfeld, C. (2012). "Lipids: a key player in the battle between the host and microorganisms." *J. Lipid Res.* 53:2487-2489.
29. Feingold KR. (2024, January 14). "Introduction to Lipids and Lipoproteins." In: Feingold KR, Anawalt B, Blackman MR, *et al.*, editors. Endotext (Internet). South Dartmouth (MA): MDText.com, Inc.; 2000–.
30. Goldstein J.L., DeBose-Boyd R.A., & Brown M.S. (2006). "Protein sensors for membrane sterols." *Cell* 124:35-46.
31. Goldstein J.L., & Brown M.S. (2009). "The LDL receptor." *Arterioscler. Thromb. Vasc. Biol.* 29:431-438.
32. Lagace T.A. (2014). "PCSK9 and LDLR degradation." *Curr. Opin. Lipidol*. 25:387-93.
33. van de Sluis B., Wijers M., & Herz J. (2017). "Lipoprotein receptors in lipoprotein metabolism." *Curr. Opin. Lipidol*. 28:241-247.
34. Wang S., Smith J.D. (2014). "ABCA1 and ABCG1: partners in cholesterol efflux." *Biofactors* 40:547-554.
35. Wang N., Yvan-Charvet, L., Lütjohann, D., Mulder, M., Vanmierlo, T., Kim, T.W., & Tall, A.R. (2008). "Cholesterol efflux pathways regulate myelopoiesis in mice." *FASEB J.* 22:1073-82.
36. Kidambi S., Patel S.B. (2008). "Lipid transporters in the human genome." *Xenobiotica*. 38:1119-1139.

37. Jia L., Betters J.L., & Yu L. (2011). "Cholesterol transport by the Niemann-Pick C1-like 1 protein." *Ann. Rev. Physiol*. 73:239-59.
38. Miksztowicz, V., Schreier, L., McCoy, M., Lucero, D., Fassio, E., Billheimer, J., Rader, D.J., & Berg, G. (2014). Role of SN1 lipases on plasma lipids in metabolic syndrome and obesity. *Arterioscler. Thromb. Vasc. Biol.*, 34:669-675.
39. Wang, H., & Eckel, R.H. (2009). Lipoprotein lipase: From gene to obesity. *Am. J. Physiol. Endocrinol. Metab.* 297:E271-E288.
40. Pirahanchi Y., Anoruo M., & Sharma S. (2023). "Lipid Metabolism Disorders." *In: StatPearls* (Internet).
41. Birrane G., Beigneux, A.P., Dwyer, B., Strack-Logue, B., Kristensen, K.K., Francone, O. L., Fong, L.G., Mertens, H.D.T., Pan, C.Q., Ploug, M., Young, S.G., & Meiyappan, M. (2019). "Structure of the lipoprotein lipase-GPIHBP1 complex that mediates plasma triglyceride hydrolysis." *Proc. Natl. Acad. Sci. U. S. A.* 116:1723-1732.
42. Kobayashi J., & Mabuchi H. (2015) "Lipoprotein lipase and atherosclerosis" *Ann. Clin. Biochem.* 52:632-637.
43. Rader D.J. (2003). "Regulation of reverse cholesterol transport and clinical implications." *Am. J. Cardiol.* 92:42J–49J.
44. Ball W.D., Hill J.W., & Scott R.J. (2012). "Basics of General, Organic, and Biological Chemistry v1.0." Pub., FlatWorld.
45. Sletten A.C., Davidson, J.W., Yagabasan, B., Moores, S., Schwaiger-Haber, M., Fujiwara, H., Gale, S., Jiang, X., Sidhu, R., Gelman, S.J., Zhao, S., Patti, G.J., Ory, D.S., & Schaffer, J.E. (2021). "Loss of SNORA73 reprograms cellular metabolism and protects against steatohepatitis." *Nat. Commun.* 12:5214.
46. Ghosh, A., Gao, L., Thakur, A., Siu, P.M., & Lai, C.W.K. (2017). "Role of free fatty acids in endothelial dysfunction. *J. Biomed. Sci.* 24:50.
47. Sherratt S.C.R., Dawoud, H., Bhatt, D.L., Malinski, T., & Mason, R.P.(2021)."Omega-3 and omega-6 fatty acids have distinct effects on endothelial fatty acid content and nitric oxide bioavailability." *Prostaglandins Leukot. Essent. Fatty Acids* 173:102337.
48. Werz O., Gerstmeier, J., Libreros, S., De la Rosa, X., Werner, M., Norris, P.C., Chiang, N., & Serhan, C.N. (2018)."Human macrophages differentially produce specific resolvin or leukotriene signals that depend on bacterial pathogenicity." *Nat. Commun.* 9:59.
49. Das U.N.(2013)."Essential fatty acids—a review." *Prostaglandins Leukot. Essent. Fatty Acids* 88:201-210.
50. Kotlyarov S., & Kotlyarova A. (2022). "Involvement of fatty acids and their metabolites in the development of inflammation in atherosclerosis." *Int. J. Mol. Sci.* 23:13084.
51. Campinho, P., Vilfan, A., & Vermot, J. (2020). "Blood flow forces in shaping the vascular system: A focus on endothelial cell behavior." *Front. Physiol*. 11:5526.
52. Boden, G. (2008). "Obesity and free fatty acids." *Endocrinol. Metab. Clin. N. Am.* 37:635-646.
53. Mathew, M., Tay, E., & Cusi, K. (2010). "Insulin resistance in nonalcoholic fatty liver disease." *Cardiovasc. Diabetol.* 9:9.
54. Pillon, N.J., Azizi, P.M., Li, Y.E., Liu, J., Wang, C., Chan, K.L., Hopperton, K.E., Bazinet, R.P., Heit, B., Bilan, P.J., Lee, W. L., & Klip, A. (2015). "Palmitate-induced inflammatory pathways in human adipose microvascular endothelial cells promote monocyte adhesion and impair insulin transcytosis." *Am. J. Physiol. Endocrinol. Metab*. 309:E35-E44.

55. Nunes Marsiglio-Librais, G., Aparecida Vilas-Boas, E., Carlein, C., Hoffmann, M.D.A., Roma, L.P., & Carpinelli, A.R. (2020). "Evidence for NADPH oxidase activation by GPR40 in pancreatic β-cells." *Redox Rep.* 25: 41-50.
56. Förstermann, U., Xia, N., & Li, H. (2017). "Roles of vascular oxidative stress and nitric oxide in cardiovascular health and disease." *Circ. Res.* 120:713-735.
57. Fukai, T., & Ushio-Fukai, M. (2011). "Superoxide dismutases: Role in redox signaling, vascular function, and diseases." *Antioxid. Redox Signal.* 15:1583-1606.
58. Yang, D., Elner, S.G., Bian, Z.M., Till, G.O., Petty, H.R., & Elner, V.M. (2007). "Pro-inflammatory cytokines increase reactive oxygen species through mitochondria and NADPH oxidase in cultured RPE cells." *Exp. Eye Res.* 85:462-472.
59. Bedard, K., & Krause, K.H. (2007). "The NOX family of ROS-generating NADPH oxidases: Physiology and pathophysiology." *Physiol. Rev.* 87:245-313.
60. Gardiner, G.J., Deffit, S.N., McLetchie, S., Pérez, L., Walline, C.C., & Blum, J.S. (2013). "A role for NADPH oxidase in antigen presentation." *Front. Immunol.* 4:295.
61. Rueckschloss, U., Duerrschmidt, N., & Morawietz, H.. (2003). "NADPH oxidase in endothelial cells: Impact on atherosclerosis." *Antioxid. Redox Signal.* 5:171-180.
62. Hamam, H.J., & Palaniyar, N. (2019). Post-translational modifications in NETosis and NETs-mediated diseases. *Biomolecules* 9:369.
63. Manea, S.A., Antonescu, M.L., Fenyo, I.M., Raicu, M., Simionescu, M., & Manea, A. (2018). "Epigenetic regulation of vascular NADPH oxidase expression and reactive oxygen species production by histone deacetylase-dependent mechanisms in experimental diabetes". *Redox Biol.* 16:332-343.
64. Panday A., Sahoo M.K., Osorio D., & Batra S. (2015). "NADPH oxidases: an overview from structure to innate immunity-associated pathologies." *Cell Mol. Immunol*. 12:5-23.
65. Flannagan R.S., Cosio G., & Grinstein S. (2009). "Antimicrobial mechanisms of phagocytes and bacterial evasion strategies." *Nat. Rev. Microbiol.* 7:355-366.
66. Sumimoto H., Miyano K., & Takeya R. (2005). "Molecular composition and regulation of the Nox family NAD(P)H oxidases." *Biochem. Biophys. Res. Commun*. 338:677-686.
67. Takeya R., Ueno, N., Kami, K., Taura, M., Kohjima, M., Izaki, T., Nunoi, H., & Sumimoto, H. (2003). "Novel human homologues of p47phox and p67phox participate in activation of superoxide-producing NADPH oxidases." *J. Biol. Chem.* 278:25234-25246.
68. Cheng G., Ritsick D., & Lambeth J.D. (2004). "Nox3 regulation by NOXO1, p47phox, and p67phox." *J. Biol. Chem.* 279:34250-34255.
69. Geiszt M., Kopp J.B., Varnai P., & Leto TL. (2000). "Identification of renox, an NAD(P)H oxidase in kidney." *Proc. Natl. Acad. Sci. U. S. A.* 97:8010-8014.
70. Gorin, Y., Ricono, J.M., Kim, N.H., Bhandari, B., Choudhury, G.G., & Abboud, H.E. (2003). "Nox4 mediates angiotensin II-induced activation of Akt/protein kinase B in mesangial cells." *Am. J. Physiol. Renal Physiol.* 285:F219-F229.
71. Lyle A.N., Deshpande, N.N., Taniyama, Y., Seidel-Rogol, B., Pounkova, L., Du, P., Papaharalambus, C., Lassègue, B., & Griendling, K.K. (2009). "Poldip2, a novel regulator of Nox4 and cytoskeletal integrity in vascular smooth muscle cells." *Circ. Res.* 105:249-259.
72. Fu, X., Beer, D.G., Behar, J., Wands, J., Lambeth, D., & Cao, W. (2006). "cAMP-response element-binding protein mediates acid-induced NADPH oxidase NOX5-S expression in Barrett's esophageal adenocarcinoma cells." *J. Biol. Chem.* 281:20368-20382.

73. De Deken, X., Wang D., Dumont J.E., & Miot F. (2002). "Characterization of ThOX proteins as components of the thyroid H_2O_2-generating system." *Exp. Cell. Res.* 273:187-196.
74. Grasberger, H., & Refetoff S. (2006). "Identification of the maturation factor for dual oxidase. Evolution of an eukaryotic operon equivalent." *J. Biol. Chem.* 281:18269-18272.
75. Ameziane-El-Hassani, R., Morand, S., Boucher, J.L., Frapart, Y.M., Apostolou, D., Agnandji, D., Gnidehou, S., Ohayon, R., Noël-Hudson, M.S., Francon, J., Lalaoui, K., Virion, A., & Dupuy, C. (2005). "Dual oxidase-2 has an intrinsic Ca^{2+}-dependent H_2O_2-generating activity." *J. Biol. Chem.* 280:30046-30054.
76. Matera, A.G., Terns R.M., & Terns M.P. (2007). "Non-coding RNAs: Lessons from the small nuclear and small nucleolar RNAs." *Nat. Rev. Mol. Cell Biol.* 8:209-220.
77. Weinstein, L.B., & Steitz J.A. (1999). "Guided tours: from precursor snoRNA to functional snoRNP." *Curr. Opin. Cell Biol.* 11:378-384.
78. Huang, Z.H., Du, Y.P., Wen, J.T., Lu, B.F., & Zhao, Y. (2022). "snoRNAs: functions and mechanisms in biological processes, and roles in tumor pathophysiology." *Cell Death Discov*. 8:259.
79. Bratkovič, T., & Rogelj, B. (2014). "Biology and applications of small nucleolar RNAs." *Biochem. Biophys. Acta*. 1839:438-443.
80. Williams, G.T., & Farzaneh, F. (2012). "Are snoRNAs and snoRNA host genes new players in cancer?" *Nat. Rev. Cancer* 12:84-8.
81. Baldini, L., Charpentier, B, & Labialle, S. (2021). "Emerging Roles of Small Nucleolar RNAs in Neurodegenerative Diseases." *Noncoding RNA* 7:30.
82. Meier, U.T. (2006). "The many facets of H/ACA ribonucleoproteins." *Trends Biochem. Sci*. 31:311-315.
83. Ganot, P., Caizergues-Ferrer, M., & Kiss T. (1997). "The family of box ACA small nucleolar RNAs is defined by an evolutionarily conserved secondary structure and ubiquitous sequence elements essential for RNA accumulation." *Genes Dev*. 11:941-956.
84. Holley, C.L., Li, M.W., Scruggs, B.S., Matkovich, S.J., Ory, D.S., & Schaffer, J. E. (2015). "Cytosolic accumulation of small nucleolar RNAs (snoRNAs) is dynamically regulated by NADPH oxidase activity." *J. Biol. Chem.* 290:11741-11748.
85. Wang, L., Gill, R., Pedersen, T.L., Higgins, L.J., Newman, J.W., & Rutledge, J.C. (2009). "Triglyceride-rich lipoprotein lipolysis releases neutral and oxidized FFAs that induce endothelial cell inflammation." *J. Lipid Res.* 50:204-213.
86. Thyagarajan, N. (2017). "Human gene array analysis of THP-1 macrophages exposed to lipoprotein hydrolysis products generated by lipoprotein lipase." Master's thesis, Memorial University of Newfoundland.
87. Lehner, R., & Verger, R. (1997). "Purification and characterization of a calcium-independent phospholipase A2 from rat liver cytosol." *Biochemistry* 36:1861-1868.
88. Pfaffl, M. W. (2001). "A new mathematical model for relative quantification in real-time RT-PCR." *Nucleic Acids Res.* 29, e45-e45.
89. Thyagarajan, N., Marshall, J.D., Pickett, A.T., Schumacher, C., Yang, Y., Christian, S.L., & Brown, R.J. (2017). "Transcriptomic analysis of thp-1 macrophages exposed to lipoprotein hydrolysis products generated by lipoprotein lipase." *Lipids* 52:189-205.

90. Rosa Neto, J. C., Calder, P. C., Curi, R., Newsholme, P., Sethi, J. K., & Silveira, L. S. (2021). "The Immunometabolic roles of various fatty acids in macrophages and lymphocytes." *Int. J. Mol. Sci.* 22:8460.
91. Ménégaut, L., Jalil, A., Thomas, C., & Masson, D. (2019). "Macrophage fatty acid metabolism and atherosclerosis: The rise of PUFAs." *Atherosclerosis* 291:52-61.
92. Ghosh, A., Gao, L., Thakur, A., Siu, P.M., & Lai, C.W.K. (2017). "Role of free fatty acids in endothelial dysfunction." *J. Biomed. Sci.* 24:50.
93. Wang, L., Gill, R., Pedersen, T.L., Higgins, L.J., Newman, J.W., & Rutledge, J.C. (2009). "Triglyceride-rich lipoprotein lipolysis releases neutral and oxidized FFAs that induce endothelial cell inflammation." *J. Lipid Res.* 50:204-213.
94. Herb, M., & Schramm, M. (2021). "Functions of ROS in macrophages and antimicrobial immunity." *Antioxidants* 10:313.
95. Canton, M., Sánchez-Rodríguez, R., Spera, I., Venegas, F.C., Favia, M., Viola, A., & Castegna, A. (2021). "Reactive oxygen species in macrophages: Sources and targets." *Front. Immunol.* 12:734229.
96. Tan, H., Wang, N., Li, S., Hong, M., Wang, X., & Feng, Y. (2016). "The reactive oxygen species in macrophage polarization: Reflecting its dual role in progression and treatment of human diseases." *Oxid. Med. Cell. Longev.* 2016:2795090.
97. Rastogi, R., Geng, X., Li, F., & Ding, Y. (2017). "NOX activation by subunit interaction and underlying mechanisms in disease." *Front. Cell. Neurosci.* 10:301.
98. Santillo, M., Colantuoni, A., Mondola P., Guida B., & Damiano S. (2015) "NOX signaling in molecular cardiovascular mechanisms involved in the blood pressure homeostasis." *Front. Physiol.* 6:194.
99. Brown, D.I., & Griendling, K.K. (2009). "Nox proteins in signal transduction." *Free Radic. Biol. Med.* 47:1239-1253.
100. Brandes, R.P., & Kreuzer, J. (2005). "Vascular NADPH oxidases: Molecular mechanisms of activation." *Cardiovasc. Res.* 65:16-27.
101. Brandes, R.P., Weissmann, N., & Schröder, K. (2014). "Nox family NADPH oxidases: Molecular mechanisms of activation." *Free Radic. Biol. Med.* 76:208-226.
102. Vermot, A., Petit-Härtlein, I., Smith, S.M.E., & Fieschi, F. (2021). "NADPH oxidases (NOX): An overview from discovery, molecular mechanisms to physiology and pathology." *Antioxidants* 10:890.
103. Cheng, G., & Lambeth, J.D. (2004). "NOXO1, regulation of lipid binding, localization, and activation of Nox1 by the Phox homology (PX) domain." *The J. Biol. Chem.* 279:4737-4742.
104. Vermot, A., Petit-Härtlein, I., Smith, S.M.E., & Fieschi, F. (2021) "NADPH oxidases (NOX): An overview from discovery, molecular mechanisms to physiology and pathology." *Antioxidants* 10:890.
105. Kawahara, T., & Lambeth, J.D. (2008). "Phosphatidylinositol (4,5)-bisphosphate modulates Nox5 localization via an N-terminal polybasic region." *Mol. Biol. Cell.* 19:4020-4031.

106. Bizouarn, T., Karimi, G., Masoud, R., Souabni, H., Machillot, P., Serfaty, X., Wien, F., Réfrégiers, M., Houée-Levin, C., & Baciou, L. (2016). "Exploring the arachidonic acid-induced structural changes in phagocyte NADPH oxidase p47(phox) and p67(phox) via thiol accessibility and SRCD spectroscopy." *FEBSJ.* 283:2896-2910.
107. Bizouarn, T., Souabni, H., Serfaty, X., Bouraoui, A., Masoud, R., Karimi, G., Houée-Levin, C., & Baciou, L. (2019). "A close-up view of the impact of arachidonic acid on the phagocyte nadph oxidase." *Methods Mol. Biol.* 1982:75-101.
108. Furukawa, T., Kurosawa, T., Mifune, Y., Inui, A., Nishimoto, H., Ueda, Y., Kataoka, T., Yamaura, K., Mukohara, S., Yoshikawa, T., Shinohara, I., Kato, T., Tanaka, S., Kusunose, M., Hoshino, Y., Matsushita, T., & Kuroda, R. (2023). "Elicitation of inhibitory effects for age-induced oxidative stress in rotator cuff-derived cells by apocynin." *Curr. Issues Mol. Bio.* 45:3434-3445.
109. Zhang, Y., Chan, M.M., Andrews, M.C., Mori, T.A., Croft, K.D., McKenzie, K.U., Schyvens, C.G., & Whitworth, J.A. (2005). "Apocynin but not allopurinol prevents and reverses adrenocorticotropic hormone-induced hypertension in the rat." *Am. J. Hypertens.* 18:910-916.
110. Kouki, A., Ferjani, W., Ghanem-Boughanmi, N., Ben-Attia, M., Dang, P.M., Souli, A., & El-Benna, J. (2023). "The NADPH oxidase inhibitors apocynin and diphenyleneiodonium protect rats from LPS-induced pulmonary inflammation." *Antioxidants* 12:770.
111. Stefanska, J., & Pawliczak, R. (2008). "Apocynin: Molecular aptitudes." *Mediators Inflamm.* 2008:106507.
112. Touyz R.M. (2008). "Apocynin, NADPH oxidase, and vascular cells: A complex matter." *Hypertension* 51:172-174.
113. Simons, J.M., Hart, B.A., Ip Vai Ching, T.R., Van Dijk, H., & Labadie, R.P. (1990). "Metabolic activation of natural phenols into selective oxidative burst agonists by activated human neutrophils." *Free Radic. Biol. Med.* 8:251-258.
114. Ximenes, V.F., Kanegae, M.P., Rissato, S.R., & Galhiane, M.S. (2007). "The oxidation of apocynin catalyzed by myeloperoxidase: proposal for NADPH oxidase inhibition." *Arch. Biochem. Biophys.* 457:134-141.
115. Siraki A.G. (2021). "The many roles of myeloperoxidase: From inflammation and immunity to biomarkers, drug metabolism and drug discovery." *Redox Biol.* 46:102109.
116. Van den Worm, E., van den Berg, A.J.J., Kemeling, G.M., Beukelman, C.J., Halkes, S.B.A., Labadie, R.P., van Dijk , H. (2001) "Isolation, characterization and activity of diapocynin, an apocynin metabolite." *Investigations on apocynin, a potent NADPH oxidase inhibitor.* Chapter 5.
117. Laleu, B., Gaggini, F., Orchard, M., Fioraso-Cartier, L., Cagnon, L., Houngninou-Molango, S., Gradia, A., Duboux, G., Merlot, C., Heitz, F., Szyndralewiez, C., & Page, P. (2010). "First in class, potent, and orally bioavailable NADPH oxidase isoform 4 (Nox4) inhibitors for the treatment of idiopathic pulmonary fibrosis." *J. Med. Chem.* 53:7715-7730.
118. Sedeek, M., Gutsol, A., Montezano, A.C., Burger, D., Nguyen Dinh Cat, A., Kennedy, C. R., Burns, K.D., Cooper, M.E., Jandeleit-Dahm, K., Page, P., Szyndralewiez, C., Heitz, F.,

Hebert, R.L., & Touyz, R.M. (2013). "Renoprotective effects of a novel Nox1/4 inhibitor in a mouse model of Type 2 diabetes." *Clin. Sci.* 124:191-202.
119. Hwang, J.S., Cha, E.H., Ha, E., Park, B., & Seo, J.H. (2020). "GKT136901 protects primary human brain microvascular endothelial cells against methamphetamine-induced blood-brain barrier dysfunction." *Life Sci.* 256:117917.
120. Schildknecht, S., Weber, A., Gerding, H.R., Pape, R., Robotta, M., Drescher, M., Marquardt, A., Daiber, A., Ferger, B., & Leist, M. (2014). "The NOX1/4 inhibitor GKT136901 as selective and direct scavenger of peroxynitrite." *Curr. Med. Chem.* 21:365-376.
121. Augsburger, F., Filippova, A., Rasti, D., Seredenina, T., Lam, M., Maghzal, G., Mahiout, Z., Jansen-Dürr, P., Knaus, U.G., Doroshow, J., Stocker, R., Krause, K.H., & Jaquet, V. (2019). "Pharmacological characterization of the seven human NOX isoforms and their inhibitors." *Redox Biol.* 26:101272.
122. Heinecke, J.W. (1999). "Is lipid peroxidation relevant to atherogenesis?" *J. Clin. Invest.* 104:135-136.
123. Leong X.F. (2021). "Lipid oxidation products on inflammation-mediated hypertension and atherosclerosis: A mini review." *Front. Nutr.* 8:717740.
124. Endale, H., Tesfaye, W., & Mengstie, T.A. (2023). "ROS induced lipid peroxidation and their role in ferroptosis." *Front. Cell Dev. Biol.* 11:1226044.
125. Wang, S., Xu, J., Zheng, J., Zhang, X., Shao, J., Zhao, L., & Hao, J. (2020). "Anti-inflammatory and antioxidant effects of acetyl-L-carnitine on atherosclerotic rats." *Med. Sci. Monit.* 26:e920250.
126. Verma, M.K., Jaiswal, A., Sharma, P., Kumar, P., & Singh, A.N. (2019). "Oxidative stress and biomarker of TNF-α, MDA and FRAP in hypertension." *J. Med. Life.* 12:253-259.
127. Serinkan Cinemre, F.B., Cinemre, H., Bahtiyar, N., Kahyaoğlu, B., Ağaç, M.T., Shundo, H., Sevinç, L., & Aydemir, B. (2021). "Apelin, omentin-1, and vaspin in patients with essential hypertension: Association of adipokines with trace elements, inflammatory cytokines, and oxidative damage markers." *Ir. J. Med. Sci.* 190:97-106.
128. Bhutia, Y., Ghosh, A., Sherpa, M.L., Pal, R., & Mohanta, P.K. (2011). "Serum malondialdehyde level: Surrogate stress marker in the Sikkimese diabetics." *J. Nat. Sci. Biol. Med.* 2:107-112.
129. Yang, R.L., Shi, Y.H., Hao, G., Li, W., & Le, G.W. (2008). "Increasing oxidative stress with progressive hyperlipidemia in human: Relation between malondialdehyde and atherogenic index." *J. Clin. Biochem. Nutr.* 43:154-158.
130. Kuznetsova, T., Prange, K.H.M., Glass, C.K., & de Winther, M.P.J. (2020). "Transcriptional and epigenetic regulation of macrophages in atherosclerosis." *Nat. Rev. Cardiol.* 17:216-228.
131. Dib, L., Koneva, L.A., Edsfeldt, A., Zurke, Y.X., Sun, J., Nitulescu, M., Attar, M., Lutgens, E., Schmidt, S., Lindholm, M.W., Choudhury, R.P., Cassimjee, I., Lee, R., Handa, A., Goncalves, I., Sansom, S.N., & Monaco, C. (2023). "Lipid-associated macrophages transition to an inflammatory state in human atherosclerosis, increasing the risk of cerebrovascular complications." *Nat. Cardiovasc. Res.* 2:656-672.

132. Chai, J.T., Ruparelia, N., Goel, A., Kyriakou, T., Biasiolli, L., Edgar, L., Handa, A., Farrall, M., Watkins, H., & Choudhury, R.P. (2018). "Differential gene expression inmacrophages from human atherosclerotic plaques shows convergence on pathways implicated by genome-wide association study risk variants." *Arterioscler. Thromb. Vasc. Biol.* 38:2718-2730.
133. Bratkovič, T., Božič, J., & Rogelj, B. (2020). "Functional diversity of small nucleolar RNAs." *Nucleic Acids Res.* 48:1627-1651.
134. Zacchini, F., Barozzi, C., Venturi, G., & Montanaro, L. (2024). "How snoRNAs can contribute to cancer at multiple levels." *NAR Cancer*, 6:zcae005.
135. Shen, L.P., Zhang, W.C., Deng, J.R., Qi, Z.H., Lin, Z.W., & Wang, Z.D. (2024). "Advances in the mechanism of small nucleolar RNA and its role in DNA damage response." *Mil. Med. Res.* 11:53.
136. Siprashvili, Z., Webster, D.E., Johnston, D., Shenoy, R.M., Ungewickell, A.J., Bhaduri, A., Flockhart, R., Zarnegar, B.J., Che, Y., Meschi, F., Puglisi, J.D., & Khavari, P.A. (2016). "The noncoding RNAs SNORD50A and SNORD50B bind K-Ras and are recurrently deleted in human cancer." *Nat. Genet.* 48:53-58.
137. Lestrade, L., & Weber, M.J. (2006) "snoRNA-LBME-db, a comprehensive database of human H/ACA and C/D box snoRNAs." *Nucleic Acids Res.* 34:D158-D162.
138. Xu, C., Bian, Z., Wang, X., Niu, N., Liu, L., Xiao, Y., Zhu, J., Huang, N., Zhang, Y., Chen, Y., Wu, Q., Sun, F., Zhu, X., & Pan, Q. (2023). "SNORA56-mediated pseudouridylation of 28 S rRNA inhibits ferroptosis and promotes colorectal cancer proliferation by enhancing GCLC translation." *J. Exp. Clin. Cancer. Res.* 42:331.
139. Daigneault, M., Preston, J.A., Marriott, H.M., Whyte, M.K., & Dockrell, D.H. (2010). "The identification of markers of macrophage differentiation in PMA-stimulated THP-1 cells and monocyte-derived macrophages." *PloS One*, 5:e8668.
140. Liu, J., Afroza, H., Rader, D.J., & Jin, W. (2010). "Angiopoietin-like protein 3 inhibits lipoprotein lipase activity through enhancing its cleavage by proprotein convertases." *J. Biol. Chem.* 285:27561-27570.
141. Lee, Y., & Siddiqui, W.J. (2023, July 24). "Cholesterol Levels." *In StatPearls[Internet]*. StatPearls Publishing. https://www.ncbi.nlm.nih.gov/books/NBK542294/
142. Tedesco, S., De Majo, F., Kim, J., Trenti, A., Trevisi, L., Fadini, G.P., Bolego, C., Zandstra, P.W., Cignarella, A., & Vitiello, L. (2018). "Convenience versus biological significance: Are PMA-differentiated THP-1 cells a reliable substitute for blood-derived macrophages when studying in vitro polarization?" *Front. Pharmacol.* 9:71.
143. Mirzaei, H., & Hamblin, M.R. (2020). "Regulation of glycolysis by non-coding RNAs in cancer: Switching on the Warburg effect." *Mol. Ther. Oncolytics.* 19:218-239.

Appendix: Supplementary figures

Figure S1

A.

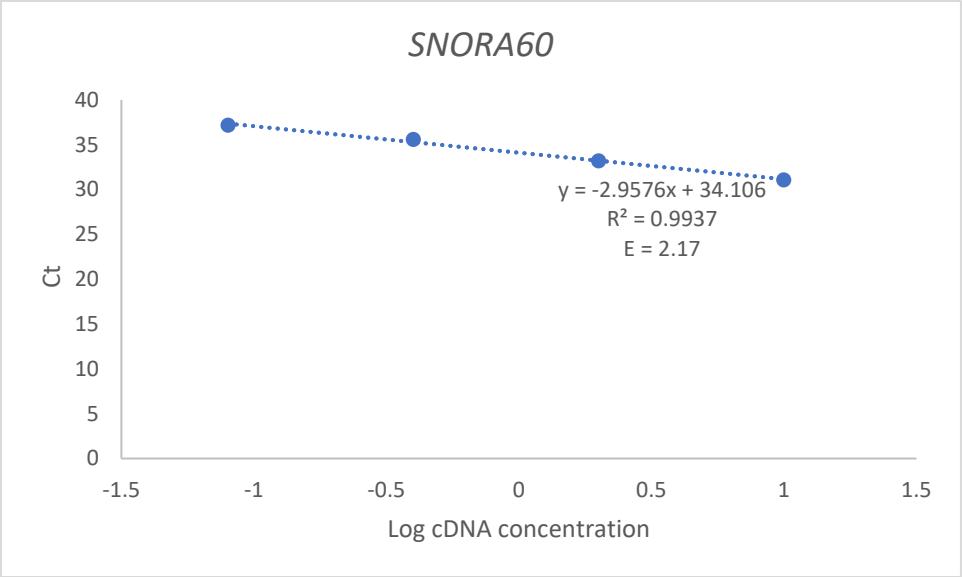
SNORA60
40
35
30
25
20
15
10
5
0
Ct
y = -2.9576x + 34.106
R² = 0.9937
E = 2.17
-1.5
-1
-0.5
0
0.5
1
1.5
Log cDNA concentration

B.

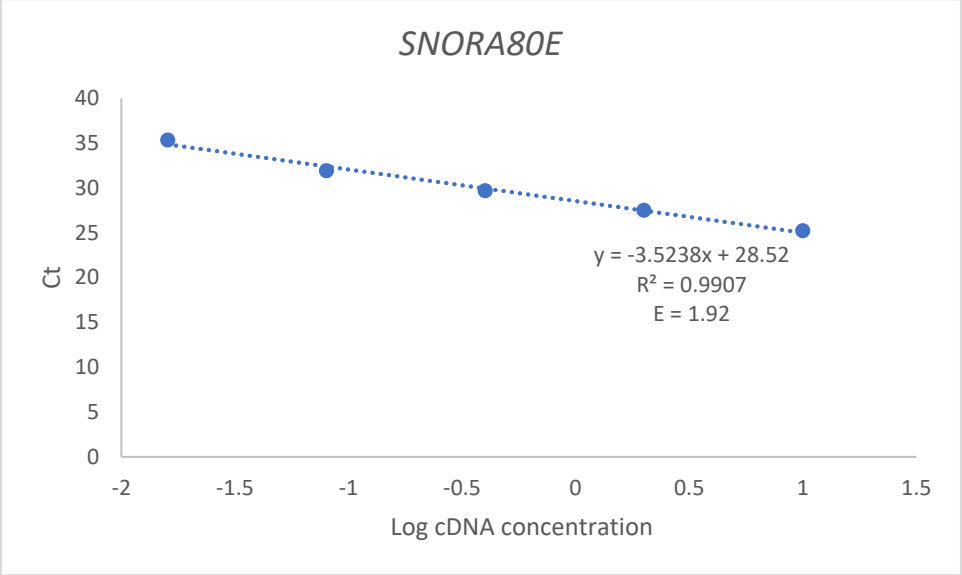
SNORA80E
40
35
30
25
20
15
10
5
0
Ct
y = -3.5238x + 28.52
R² = 0.9907
E = 1.92
-2
-1.5
-1
-0.5
0
0.5
1
1.5
Log cDNA concentration

C.

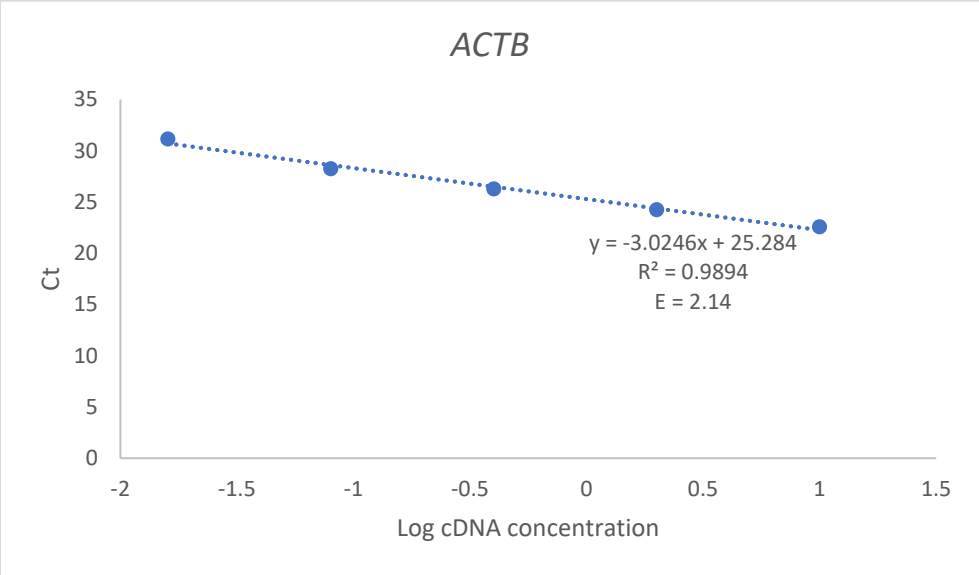

Figure S1: Amplification efficiency standard curves

Standard curves used for calculating amplification efficiencies of A. SNORA60, B. SNORA80E, and C. ACTB. The amplification efficiencies (E) of the primer pair for SNORA60, SNORA80E, and ACTB were calculated by plotting the threshold cycle (Ct) values for each gene against Log cDNA concentrations (10, 2, 0.4, 0.08, and 0.016 ng) of the sample. Amplification efficiency was calculated using the slope from the standard curve.

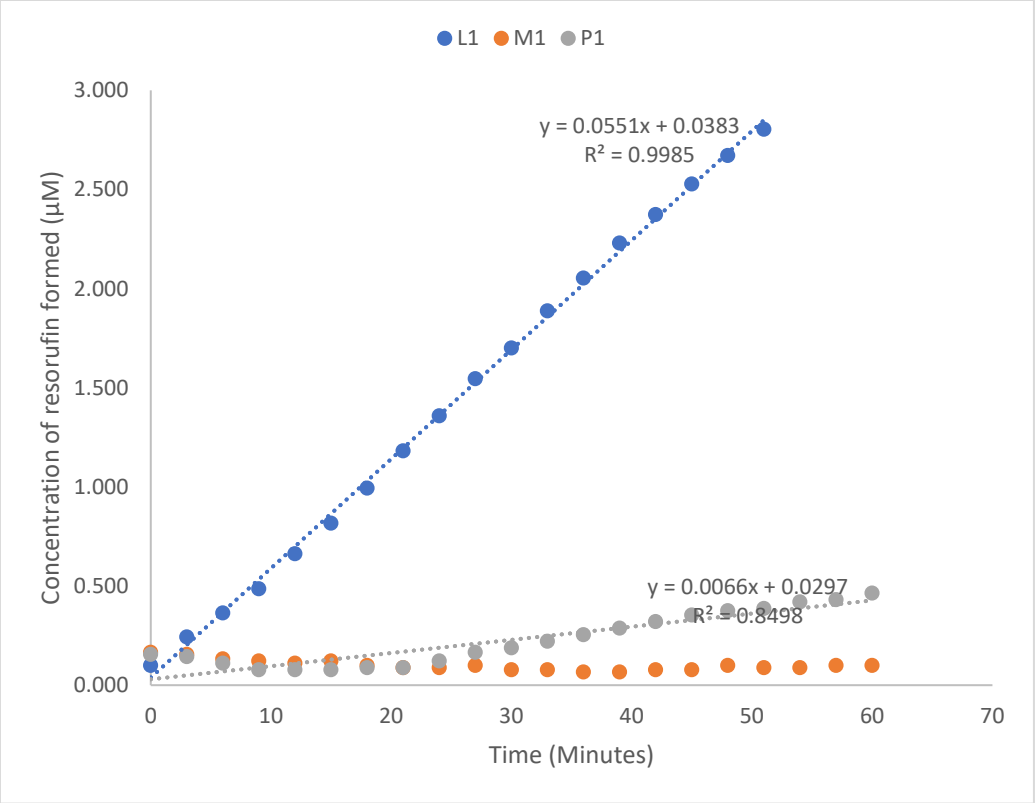

Figure S2: Lipoprotein lipase activity graph.

Graph showing the rate of resorufin formation in heparinized media sample collected from HEK293 cells transfected with either pcDNA3.LPL(L1) or empty vector pcDNA3 (P1), and from non-transfected HEK293 cells (M1). The slope of the graph was used to calculate LPL activity in the samples.